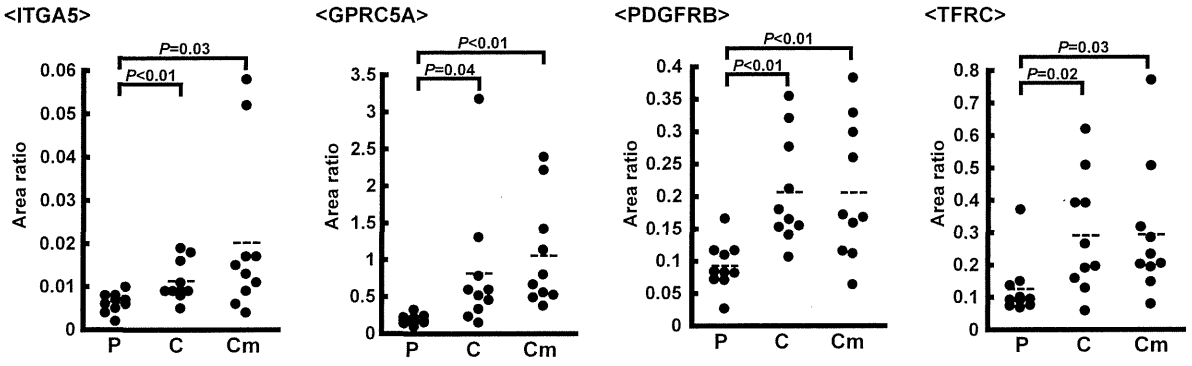
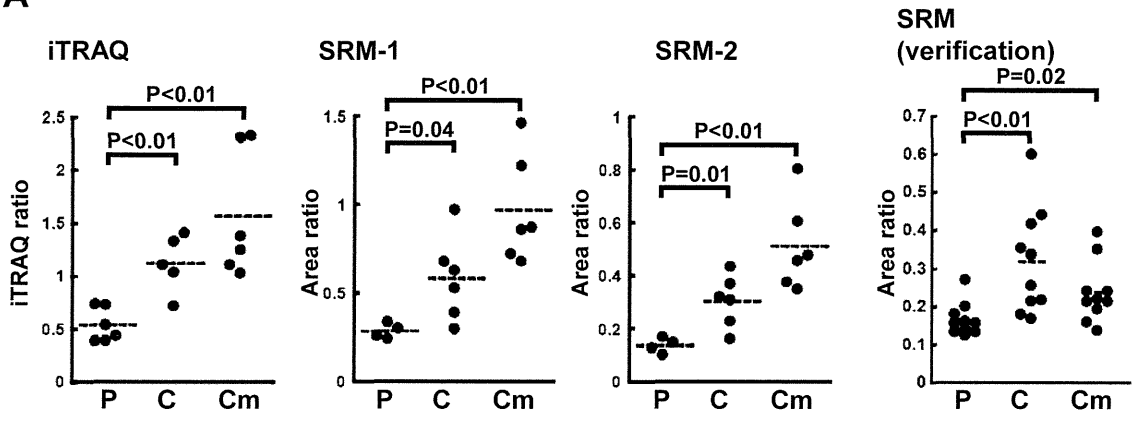
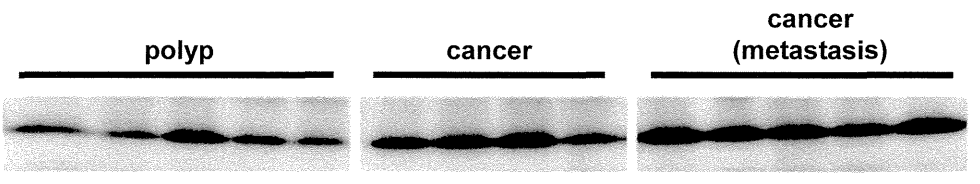

<ITGA5>
P=0.03
P<0.01
Area ratio
0.06
0.05
0.04
0.03
0.02
0.01
0
P
C
Cm
<GPRC5A>
P<0.01
P=0.04
Area ratio
3.5
3
2.5
2
1.5
1
0.5
0
P
C
Cm
<PDGFRB>
P<0.01
P<0.01
Area ratio
0.4
0.35
0.3
0.25
0.2
0.15
0.1
0.05
0
P
C
Cm
<TFRC>
P=0.03
P=0.02
Area ratio
0.8
0.7
0.6
0.5
0.4
0.3
0.2
0.1
0
P
C
Cm

Figure 3

A


iTRAQ
SRM-1
SRM-2
SRM (verification)
iTRAQ ratio
Area ratio
P<0.01
P<0.01
P<0.01
P=0.04
P<0.01
P=0.01
P=0.02
P<0.01
P C Cm

B


polyp
cancer
cancer (metastasis)

C

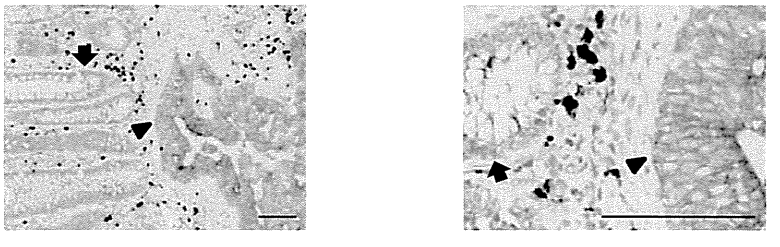

Bars, 100 μm

Figure 4

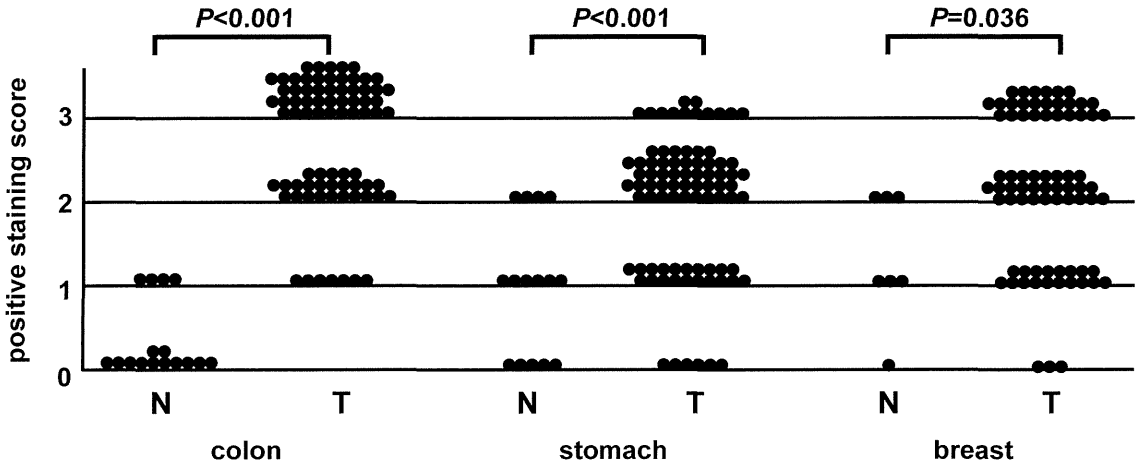

P<0.001
P<0.001
P=0.036
positive staining score
3
2
1
0
N
T
N
T
N
T
colon
stomach
breast

Figure 5

OPEN

Citation: Oncogenesis (2014) 3, e94; doi:10.1038/oncsis.2014.6
© 2014 Macmillan Publishers Limited All rights reserved 2157-9024/14
www.nature.com/oncsis

ORIGINAL ARTICLE

Lamin B2 prevents chromosome instability by ensuring proper mitotic chromosome segregation

T Kuga[1,2,3], H Nie[2], T Kazami[2], M Satoh[2], K Matsushita[2], F Nomura[2], K Maeshima[4], Y Nakayama[3] and T Tomonaga[1,2]

The majority of human cancer shows chromosomal instability (CIN). Although the precise mechanism remains largely uncertain, proper progression of mitosis is crucial. B-type lamins were suggested to be components of the spindle matrix of mitotic cells and to be involved in mitotic spindle assembly; thus, B-type lamins may contribute to the maintenance of chromosome integrity. Here, using a proteomic approach, we identified lamin B2 as a novel protein involved in CIN. Lamin B2 expression decreased in colorectal cancer cell lines exhibiting CIN, as compared with colorectal cancer cell lines exhibiting microsatellite instability (MIN), which is mutually exclusive to CIN. Importantly, lamin B2 knockdown in MIN-type colorectal cancer cells induced CIN phenotypes such as aneuploidy, chromosome mis-segregation and aberrant spindle assembly, whereas ectopic expression of lamin B2 in CIN-type colorectal cancer cells prevented their CIN phenotypes. Additionally, immunohistochemical analysis showed a lower expression of lamin B2 in cancer tissues extracted from patients with sporadic colorectal cancer (CIN-type) than that from patients with hereditary non-polyposis colorectal cancer (HNPCC; MIN type). Intriguingly, mitotic lamin B2 in MIN cancer cells was localized outside the spindle poles and mitotic lamin B2 localization was diminished in CIN cancer cells, suggesting an important role of lamin B2 in proper mitotic spindle formation. The obtained results suggest that lamin B2 maintains chromosome integrity by ensuring proper spindle assembly and that its downregulation causes CIN in colorectal cancer.

Oncogenesis (2014) **3,** e94; doi:10.1038/oncsis.2014.6; published online 17 March 2014

Subject Categories: Molecular oncology

Keywords: colorectal cancer; chromosomal instability; lamin B2; chromosome segregation; mitotic spindle

INTRODUCTION

Cancer is widely accepted as a disease of genetic instability. This instability exists as two distinct forms: chromosomal instability (CIN), characterized by gains or losses of whole or large portions of chromosomes, and microsatellite instability (MIN), characterized by mutations at the nucleotide level.[1–3] The fact that most cancers have abnormal chromosomal content, called aneuploidy, indicates that CIN has an important role in carcinogenesis.[4]

CIN has been recognized to occur as a result of chromosome mis-segregation, which is caused by defects in mitotic functions, such as chromosome condensation, sister-chromatid cohesion, kinetochore structure, centrosome formation and microtubule dynamics, as well as the mitotic checkpoint that monitors the proper progression of mitosis.[4] Several proteins involved in mitotic processes have been shown to have mutated or altered expression levels in cancer.[5–8] Moreover, we previously showed that core kinetochore proteins, CENP-A and CENP-H, are overexpressed in colorectal cancer and involved in CIN,[9–11] suggesting that nuclear proteins are also responsible for chromosome integrity.

Nuclear lamins were initially identified as the major components of the nuclear lamina, a proteinaceous layer found at the interface between chromatin and inner nuclear membrane.[12] Although the early view of lamins was as a static nuclear skeleton, recent observations suggest that lamins have far more active roles throughout the cell cycle, such as DNA replication, transcription and several mitotic events.[13–23] Lamins are grouped as A type (lamins A and C) or B type (lamins B1 and B2) on the basis of their biochemical properties and behavior during mitosis.[24] B-type lamins are expressed in all somatic cell types, whereas A-type lamins are expressed primarily in differentiated cells.[24]

During mitosis, B-type lamin has been observed to associate with the mitotic spindle[25,26] and shown to have an important role in mitotic spindle formation.[14,21] Both depletion and a dominant-negative mutant of lamin B proteins disrupted spindle assembly in mitosis.[21] In *C. elegans*, downregulation of lamin expression induced gross mitotic defects, such as anaphase chromosome 'bridges' and unequal distribution of chromatin to daughter cells.[13] These observations suggest that B-type lamins have an important role in proper chromosome segregation.

In this study, we searched for CIN-related proteins using a proteomic approach and showed the important role of lamin B2 in CIN by manipulating its expression levels in CIN and MIN colorectal cancer cell lines. Moreover, we observed a decreased expression of lamin B2 in human sporadic colorectal cancer tissues (CIN type) as compared with hereditary non-polyposis colorectal cancer tissues (HNPCC, MIN type). Additionally, by dissecting mitotic localization of lamin B2, we suggested a novel mechanism of how lamin B2 maintains mitotic spindle assembly to prevent CIN.

[1]Laboratory of Proteome Research, National Institute of Biomedical Innovation, Osaka, Japan; [2]Department of Molecular Diagnosis (F8), Graduate School of Medicine, Chiba University, Chiba, Japan; [3]Department of Biochemistry and Molecular Biology, Kyoto Pharmaceutical University, Kyoto, Japan and [4]Biological Macromolecules Laboratory, Structural Biology Center, National Institute of Genetics, Shizuoka, Japan. Correspondence: Professor T Tomonaga, Laboratory of Proteome Research, National Institute of Biomedical Innovation, 7-6-8 Saito-Asagi, Ibaraki567-0085, Osaka, Japan.
E-mail: tomonaga@nibio.go.jp
Received 25 May 2013; revised 27 December 2013; accepted 27 January 2014

RESULTS

Proteomic analysis of colorectal cancer cell lines reveals that lamin B2 is downregulated in CIN cell lines

To search for the factors involved in CIN, we compared protein expression profiles of CIN and MIN colorectal cancer cell lines by a proteomic approach. Both types of cell lines have previously been well studied;[1,27] thus, we used HT29, SW480, SW837 and Caco-2 as CIN cell lines and HCT116, RKO, DLD1 and SW48 as MIN cell lines. Nuclear proteins were extracted from each cell line. Pooled nuclear extracts of CIN cell lines were labeled with Cy5 dyes, whereas those of MIN cell lines were labeled with Cy3 dyes. The labeled proteins were mixed and separated in the same agarose two-dimensional electrophoresis gel (Figure 1a). Proteins that increased or decreased in CIN nuclear extracts (displayed as red or green spots, respectively) were identified by tandem mass spectrometry and their expression levels were validated by western blotting.

One of the clearest differences in expression between CIN and MIN nuclear extracts was that of lamin B2, which significantly decreased in all tested CIN cell lines as compared with MIN cell lines (Figures 1a, arrow and b). In contrast, lamin B1 did not show a clear difference between CIN and MIN cell lines, and the expression of lamin A/C varied between individual cell lines (Figure 1b). Immunofluorescence for lamin B2 further confirmed the decreased level of lamin B2 in CIN cell lines. Although strong lamin B2 staining was detected at the nuclear envelope in several MIN cell lines, the staining was very slight in CIN cell lines (Figure 1c). Thus, these results indicate that the expression of lamin B2 is specifically suppressed in CIN cell lines.

Repression of lamin B2 in MIN cancer cells causes aneuploidy

To examine whether the decreased expression of lamin B2 was involved in CIN, MIN-type HCT116 cells were transfected with lamin B2-siRNA and analyzed for alterations in the chromosome number by fluorescent in situ hybridization (FISH) analysis using several centromere probes (CEPs). Depletion of lamin B2 was checked by western blotting (Figure 2a, lanes 1 and 2) and reverse transcription (RT)–PCR (Supplementary Figure S1). Figure 2b shows that lamin B2 knockdown increased the number of aneuploid cells (arrows). As assessed by counting the number of centromere signals for chromosomes 7, 8, 12 and 15 in at least 200 nuclei, the frequency of aneuploid cells increased 2.2–4.4 times in lamin B2-siRNA-treated cells as compared with control cells (Figure 2c). Similar results were obtained using another lamin B2-siRNA targeting a different region of lamin B2 mRNA (Supplementary Figure S2).

To exclude the possibility that the aneuploidy observed above was due to the off-target effect of lamin B2-siRNA, HCT116 cells were co-transfected with lamin B2-siRNA and lamin B2-GFP plasmid, which would replace the expression and function of endogenous lamin B2. The expression level of lamin B2-GFP was comparable to that of endogenous lamin B2 (Figure 2a). The number of aneuploid cells was then evaluated. By transfection with lamin B2-GFP, the frequency of aneuploidy was markedly decreased as compared with that in cells treated with lamin B2-siRNA alone, and it was almost comparable to that of control-siRNA-treated cells (Figure 2c). These results indicate that the suppression of lamin B2 causes aneuploidy.

To examine the effect of lamin B2 stable knockdown on the proliferation and CIN of cancer cells, we attempted to generate HCT116 MIN cell lines stably depleted of lamin B2 using four plasmids encoding different lamin B2-shRNA. We could obtain only one clone exhibiting ~60–70% depletion of lamin B2 (Supplementary Figure S3a). This clone showed neither increased frequency of aneuploidy (Supplementary Figure S3b) nor alteration in cell proliferation (data not shown). These results suggest that this incomplete depletion of lamin B2 may not be satisfactory to cause CIN, and that a certain level of lamin B2 is sufficient to maintain chromosome integrity. Because MIN cell lines maintain the checkpoint system against aneuploidy,[28] HCT116 cells depleted of lamin B2 at sufficient levels to cause CIN might be lost by cell death or cell-cycle arrest during the clonal selection. Further study using other approaches is also needed to understand the effects of CIN caused by lamin B2 depletion on cancer survival.

Repression of lamin B2 in MIN cancer cells causes mitotic delay and chromosome mis-segregation

To further examine whether the aneuploidy observed by the depletion of lamin B2 occurred as the result of chromosome mis-segregation, HCT116 cells expressing histone H2B-GFP were treated with lamin B2-siRNA and live-cell imaging of the mitosis was carried out. The duration of mitosis in lamin B2-siRNA-treated cells was significantly longer than in control cells. Compared with control cells that took 12.5 ± 5.6 min from congression to separation of sister chromatids, lamin B2-siRNA-treated cells took more than two times longer (28.9 ± 18.2 min; Student's *t*-test; $P = 2 \times 10^{-12}$) to complete metaphase (Figure 2d; Supplementary Figure S4; Supplementary Videos 1 and 2). Moreover, lamin B2-depleted cells often showed signs of chromosome mis-segregation, such as chromosome bridges and lagging chromosomes (Figure 2d, arrowheads). These results strongly suggest that lamin B2 is involved in proper chromosome segregation.

Repression of lamin B2 in MIN cancer cells compromises mitotic spindle formation

What is the mechanism of the aberrant mitosis induced by suppression of lamin B2 expression? Recent reports showed that B-type lamins are required for spindle assembly;[14,21] thus, to test the hypothesis that suppression of lamin B2 in MIN cancer cells induces abnormal spindle assembly, two MIN cell lines, HCT116 and RKO, were transfected with lamin B2-siRNA and examined by immunofluorescence with antibodies against α- and β-tubulin, components of the mitotic spindle. For accumulation of mitotic cells, 48 h after transfection, cells were synchronized with thymidine for 16 h and then cultured in fresh medium for 10–12 h. Depletion of lamin B2 caused a spindle defect or poor spindle morphology with a lack of chromosome congression, whereas control cells showed clear mitotic spindles (Figures 3a and b). Suppression of lamin B2 in HCT116 cells caused an increase in the spindle defect to 40.6% as compared with 16.0% of control cells ($n = 50$–100 mitotic cells). These results suggest that depletion of lamin B2 induces mitotic defects, mainly due to aberrant spindle assembly.

Ectopic expression of lamin B2 in CIN cancer cells prevents chromosome mis-segregation and severe aneuploidy

We next examined whether the induction of lamin B2 expression in CIN cancer cells could rescue the mitotic defects characteristic of CIN. CIN-type WiDr cells expressing histone H2B-GFP were transfected with lamin B2-mCherry and live-cell imaging of mitosis was carried out. Expression of lamin B2-mCherry was confirmed by western blotting (Figure 4a) and fluorescence microscopy (Figure 4b). Cells transfected with the control plasmid encoding mCherry alone exhibited chromosome bridges or lagging chromosomes in anaphase at high frequency (38.1%) (Figure 4b; Supplementary Video 3). In addition, these cells showed severe mitotic delay, 166 ± 125 min from nuclear envelope breakdown to anaphase onset (Figure 4c). Strikingly, ectopic expression of lamin B2-mCherry not only decreased the frequency of anaphase chromosome mis-segregation (24.4%) but significantly improved mitotic delay (75 ± 24 min) (Figures 4b and c; Supplementary Video 4). These results suggest that lamin B2 re-expression promotes accurate chromosome congression and prevents chromosome mis-segregation.

© 2014 Macmillan Publishers Limited

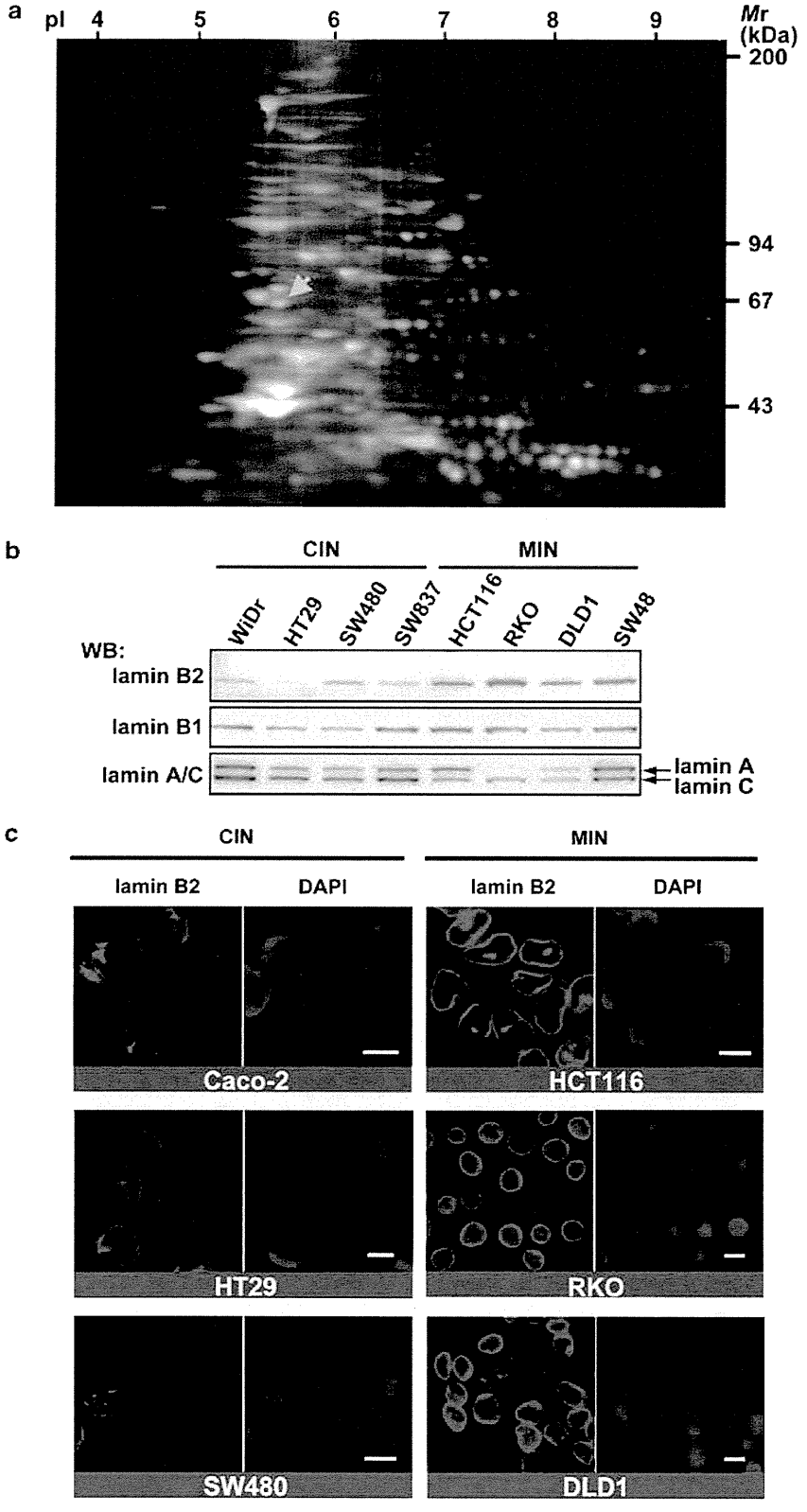


Figure 1. Proteomic analysis of colorectal cancer cell lines revealed that lamin B2 is downregulated in CIN cell lines. (**a**) Proteomic analysis of CIN and MIN cell lines using agarose 2D-DIGE. Nuclear extracts prepared from the cell lines were labeled with Cy3 (MIN) and Cy5 (CIN), and separated with two-dimensional electrophoresis. Increased and decreased protein spots in CIN nuclei are displayed as red (Cy5) and green (Cy3), respectively. Yellow arrow shows the protein spot corresponding to lamin B2. (**b**) Western blot analysis of nuclear extracts (10 μg) from CIN and MIN cell lines using antibodies to lamin B2, B1 and lamin A/C. (**c**) Immunostaining of CIN and MIN cell lines using anti-lamin B2 antibody and DAPI for DNA. Images show interphase cells. Scale bars, 10 μm.

© 2014 Macmillan Publishers Limited

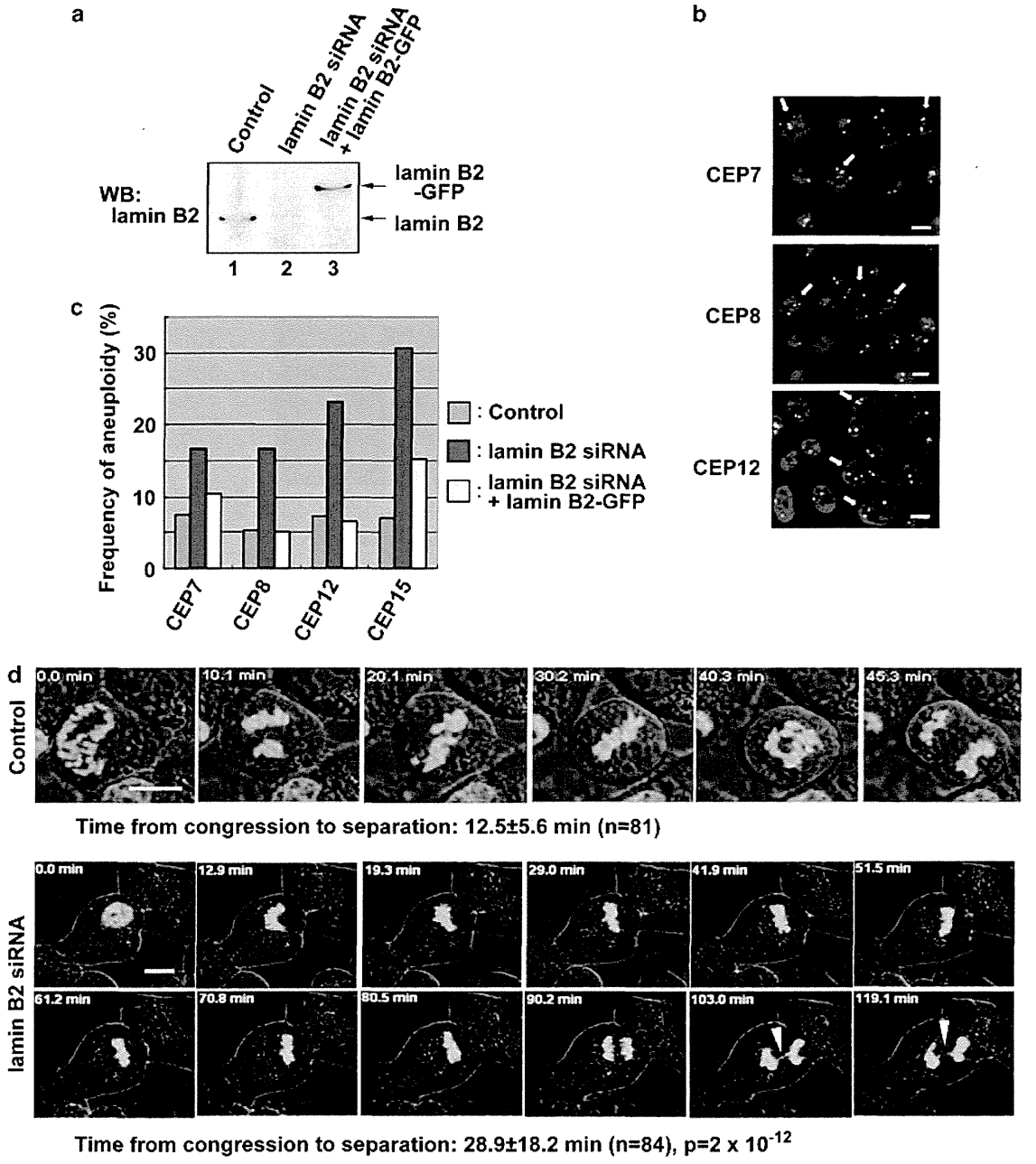


Figure 2. Repression of lamin B2 induces mitotic defects and aneuploidy. (**a**) Lamin B2-siRNA alone or together with lamin B2-GFP expression plasmid was transfected into MIN-type HCT116 cells and, 48 h later, the expressions of lamin B2 and lamin B2-GFP were checked by western blotting. Lane 1, control-siRNA; lane 2, lamin B2-siRNA alone; lane 3, lamin B2-siRNA + lamin B2-GFP expression plasmid. (**b**) FISH analysis using centromere probes (CEP7, 8 and 12) was performed 48 h after transfection with lamin B2-siRNA in HCT116 cells. White arrows indicate aneuploid cells. (**c**) Frequency of aneuploid cells in HCT116 cells transfected with either lamin B2-siRNA alone or together with lamin B2-GFP expression plasmid. Centromere singles (CEP7, 8, 12 and 15) were counted in at least 200 cells. (**d**) HCT116 cells stably expressing histone H2B-GFP were treated with control or lamin B2-siRNA for 24 h. Time-lapse images of the cells were taken at 3- to 5-min intervals. Images shown are representative of control or lamin B2-siRNA-treated cells from prophase to anaphase. Control cells took 12.5 ± 5.6 min ($n = 81$) from congression to separation of sister chromatids, whereas lamin B2-siRNA-treated cells took 28.9 ± 18.2 min ($n = 84$). Arrowheads indicate a chromosomal bridge. Scale bars, 10 μm.

We next examined aneuploidy in lamin B2-overexpressed CIN cells. WiDr cells were transfected with lamin B2-GFP or GFP alone (control) and, 7 days after transfection, analyzed by FISH with CEP12 and 15. A large fraction of control cells exhibited three copies of CEP12 and 15 signals, whereas 9.5 ± 1.5% and 14.5 ± 2.5% of control cells exhibited ⩾4 copies of CEP12 and 15 signals, respectively (Figures 4d and e). Strikingly, ectopic expression of lamin B2-GFP decreased the number of severely aneuploid cells exhibiting ⩾4 copies of CEP12 (6.0 ± 4.7%) and CEP15 (4.6 ± 1.5%) signals, while the number of cells exhibiting 3 copies of these CEP signals increased (Figures 4d and e). Given that intercellular heterogeneity in the chromosome copy number is a typical feature of CIN cancer cells,[1,28] these results suggest that lamin B2 overexpression improves chromosome integrity.

© 2014 Macmillan Publishers Limited

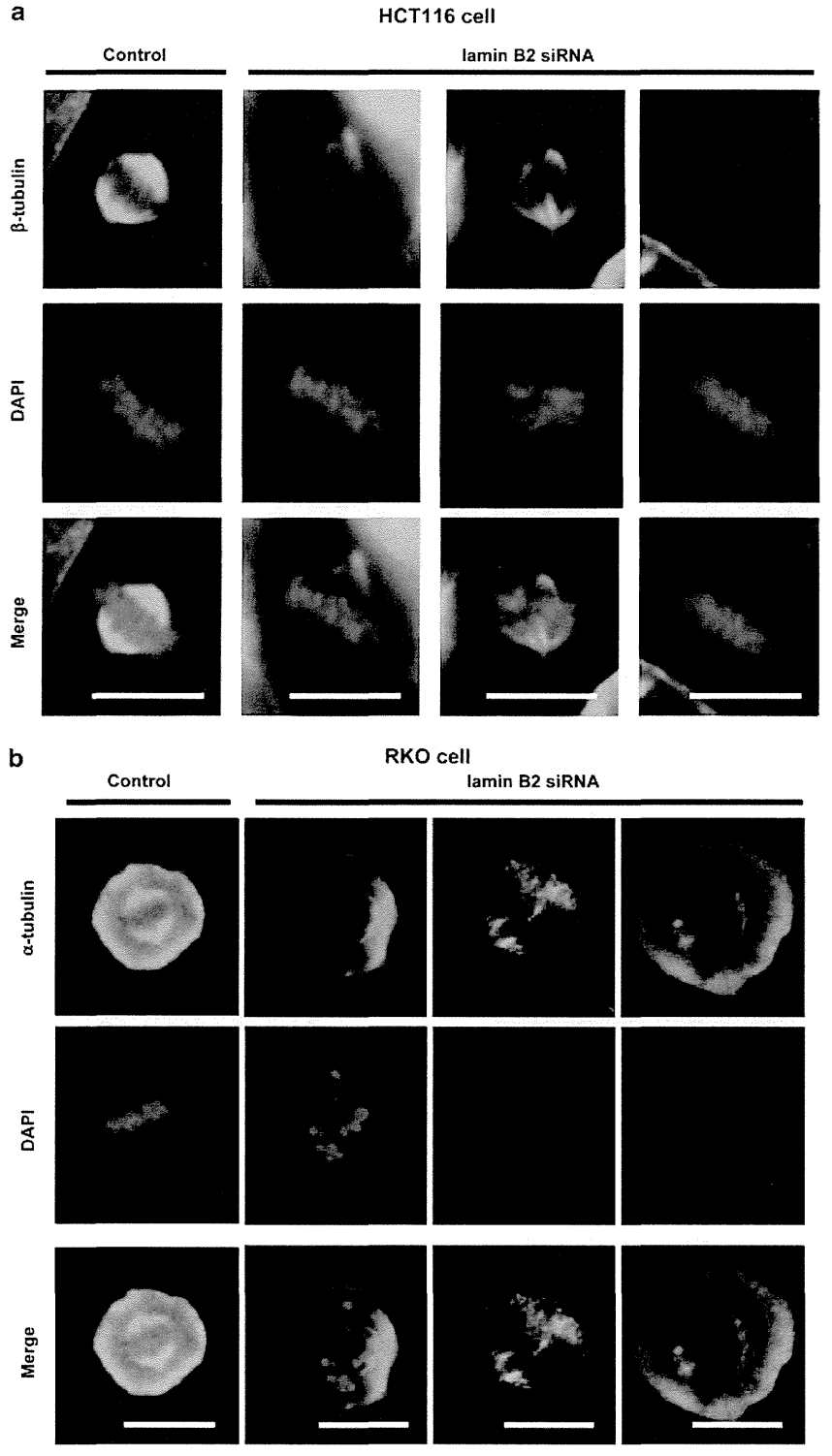


Figure 3. Repression of lamin B2 abrogates mitotic spindle formation. MIN cell lines, HCT116 and RKO, were transfected with control- or lamin B2-siRNA. Forty-eight hours after transfection, the cells were synchronized with thymidine for 16 h and then released into fresh medium. Cells that entered mitosis were analyzed by immunostaining using anti-β-tubulin (**a**) and α-tubulin (**b**) antibodies in HCT116 (**a**) and RKO (**b**) cells, respectively. DNA was marked by DAPI. Scale bars, 10 μm.

Ectopic expression of lamin B2 in CIN cancer cells prevents aberrant mitotic spindle formation

We further examined mitotic spindle formation in CIN cancer cells with overexpression of lamin B2. To monitor mitotic spindle formation, we generated WiDr cells stably expressing mCherry-α-tubulin. The cells were transfected with lamin B2-GFP or GFP (control) and live-cell imaging of mitosis was carried out. Control cells showed poor spindle morphology at high frequency (38.0%) during chromosome segregation (Figure 5; Supplementary Video 5), suggesting that mitotic spindle formation is disturbed

© 2014 Macmillan Publishers Limited

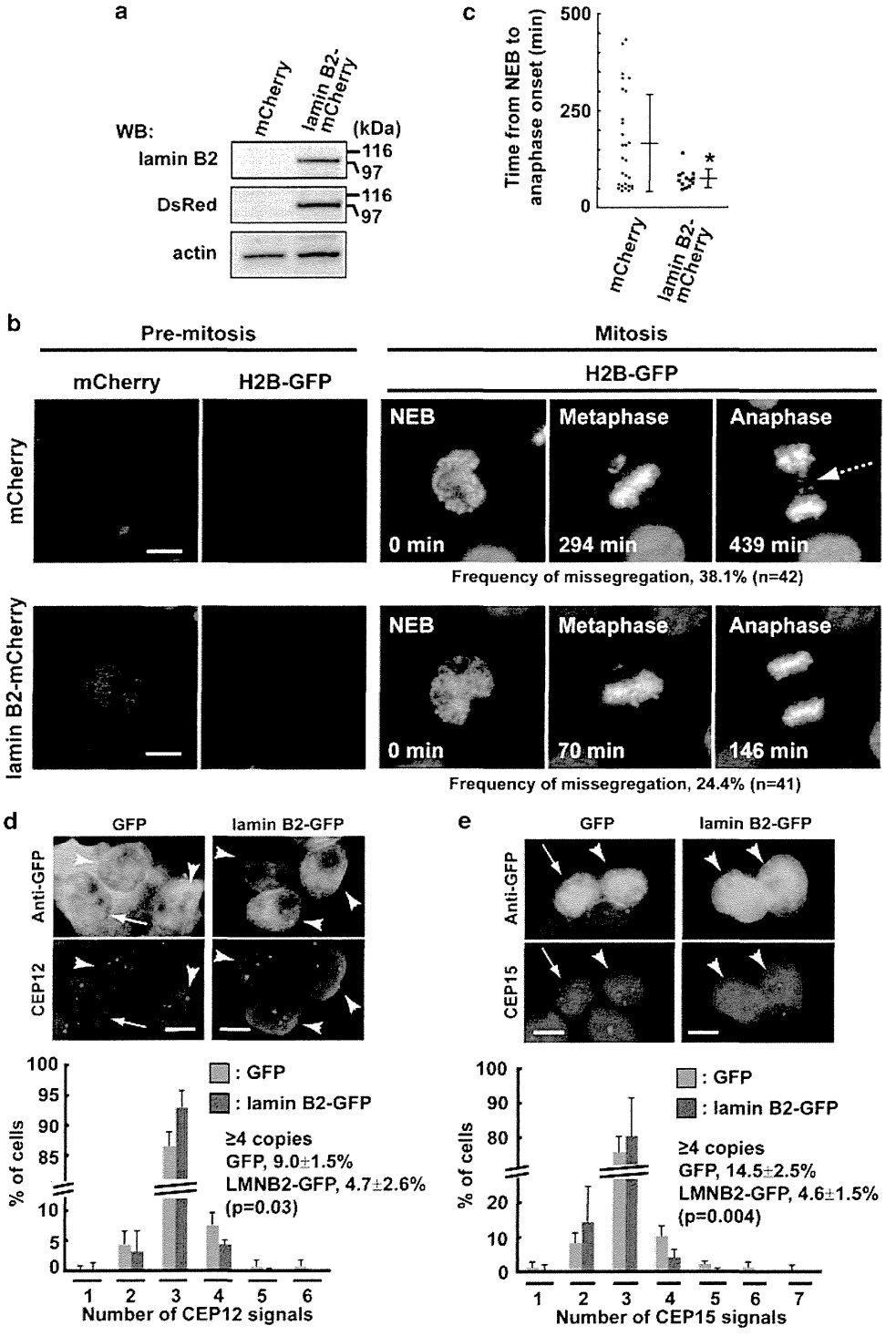


Figure 4. Ectopic expression of lamin B2 in CIN cancer cells prevents mitotic defects. (**a**–**c**) WiDr cells stably expressing histone H2B-GFP were transfected with lamin B2-mCherry or mCherry (control) expression plasmid, and expression of lamin B2-mCherry (M_r, 96 kDa) was examined by western blotting with anti-lamin B2 and anti-DsRed antibodies (**a**). Anti-DsRed antibody can detect mCherry. Living cells expressing lamin B2-mCherry or mCherry were monitored by confocal microscopy. Representative images of living cells are shown (**b**). Elapsed times from nuclear envelope breakdown (NEB) are indicated at the bottom of mitotic images (**b**). Dotted arrow indicates chromosome mis-segregation in anaphase. Scale bars, 10 μm. Percentages of cells exhibiting chromosome mis-segregation during anaphase (mCherry, $n = 42$; lamin B2-mCherry, $n = 41$) are indicated below mitotic images (**b**). (**c**) Plot represents the value of the time from NEB to anaphase onset in each cell, and the means ± s.d. are shown (mCherry, $n = 28$; lamin B2-mCherry, $n = 13$). Asterisk indicates a significant difference from the control, calculated by Student's *t*-test (*$P < 0.05$). (**d**, **e**) CIN-type WiDr cells were transfected with lamin B2-GFP or GFP (control) expression plasmid. Seven days after transfection, cells were analyzed by immunofluorescence with anti-GFP antibody and FISH with CEP12 (**d**) or CEP15 (**e**). DNA was marked by DAPI. Projections of z-stack images at 1-μm intervals are shown. Arrowheads and arrows indicate cells exhibiting 3 and ⩾4 copies of CEP signals, respectively. Scale bars, 10 μm. Bar diagrams show percentages of cells exhibiting indicated copies of CEP12 (**d**) or CEP15 (**e**) signals. Data are the mean ± s.d. of four (**d**) or three (**e**) independent experiments ($n > 100$ cells for each experiment). The percentage of cells exhibiting ⩾4 copies of CEP12 (**d**) or CEP15 (**e**) signals significantly decreased upon lamin B2 ectopic expression (Student's *t*-test).

© 2014 Macmillan Publishers Limited

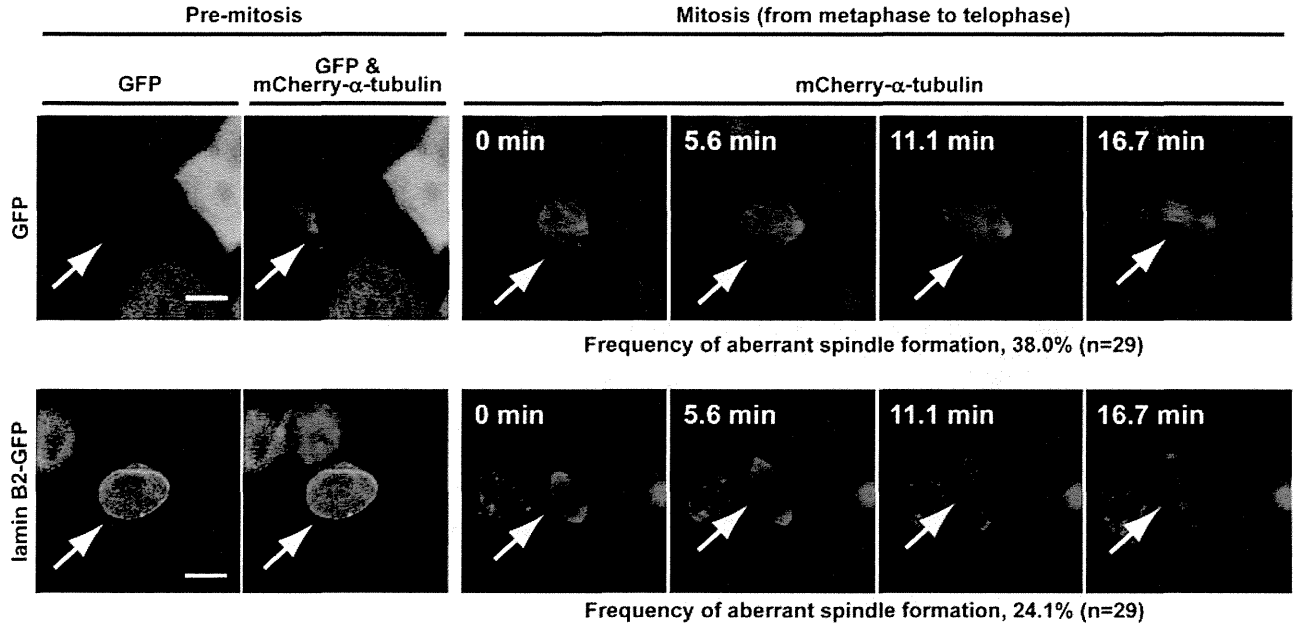


Figure 5. Ectopic expression of lamin B2 in CIN cancer cells prevents aberrant mitotic spindle formation. WiDr cells stably expressing mCherry-α-tubulin were transfected with lamin B2-GFP or GFP (control) expression plasmid. Living cells expressing lamin B2-GFP or GFP were monitored by confocal microscopy. Images shown are representative cells (arrows). Scale bars, 10 μm. Elapsed times during chromosome segregation are indicated at the top of mitotic images. Percentages of cells exhibiting aberrant spindle formation during mitosis (GFP, $n = 29$; lamin B2-GFP, $n = 29$) are indicated below mitotic images.

in WiDr cells. In lamin B2-GFP-expressing cells, the frequency of poor spindle morphology was reduced (24.1%) (Figure 5; Supplementary Video 6). These results suggest that lamin B2 overexpression improves the accuracy of chromosome segregation by preventing aberrant mitotic spindle formation.

Mitotic lamin B2 localization outside the spindle poles disappears in CIN cancer cells

Previous reports suggested that B-type lamins are structural components of the mitotic spindle matrix required to promote spindle assembly.[21] To visualize mitotic lamin B2 in CIN and MIN cell lines, we performed immunofluorescence with anti-lamin B2 antibody. Although HCT116 and DLD1 MIN lines exhibited intensive staining for mitotic lamin B2 around the spindle poles, SW837 and HT29 CIN lines showed no or very weak staining for mitotic lamin B2 (Figure 6a). These results suggest that CIN cancer cells largely lose the mitotic function of lamin B2.

Unexpectedly, lamin B2 in MIN colorectal cancer cell lines was distributed mainly outside the spindle poles (Figure 6a, magnified images), although the previous report showed co-localization of lamin B2 with kinetochore microtubules in mitotic HeLa cells.[21] Staining of mitotic lamin B2 in HCT116 MIN cells was detected using both rabbit (Figure 6a) and mouse (Figure 6b) anti-lamin B2 antibodies and disappeared upon treatment with lamin B2-siRNA (Figure 6b), confirming the specificity of mitotic lamin B2 staining. Lamin B1 was also localized outside spindle poles, but more broadly than lamin B2. Lamin A/C showed uniform staining throughout the cytoplasm (Figures 6c and d). The specificity of lamins B1 and A/C staining was also confirmed by their knock-down (Figures 6c and d). The mitotic lamin B3 matrix formed in Xenopus egg extracts contained spindle assembly factors, including Eg5[21]; however, in HCT116 cells, a large fraction of lamin B2 was not co-localized with Eg5 (Figure 6e). Taken together, these results suggest that the disappearance of mitotic lamin B2 outside the spindle poles is involved in aberrant spindle assembly and chromosome mis-segregation.

SUN1 is a protein associated with mitotic lamin B2

To further understand the role of lamin B2 in spindle formation, we identified proteins associated with lamin B2 in mitosis. Immunoprecipitates using anti-lamin B2, B1 or A/C antibody were prepared from mitotic HCT116 MIN cells and analyzed by LC-MS/MS. By comparing proteins identified from lamin B2 immunoprecipitates with those of lamin B1 and A/C immunoprecipitates, SUN1, an inner nuclear membrane protein,[29,30] was determined as a mitotic lamin B2-associated protein (Supplementary Table S1). In mitotic HCT116 cells, SUN1 was colocalized with lamin B2 and SUN1 staining was attenuated upon knockdown of SUN1 (Figure 6f), indicating that SUN1 is associated with mitotic lamin B2 outside the spindle poles. Since lamins and SUN1 were reported to be involved in stabilizing the position of the nucleus in the cell,[31,32] these results suggest that lamin B2 and SUN1 may contribute to mitotic spindle formation by physically supporting the spindle poles.

Sporadic colorectal cancer tissues (CIN) show decreased lamin B2 expression

The majority of human sporadic colorectal cancer exhibits CIN, whereas HNPCC exhibits MIN.[33] We therefore compared the lamin B2 expression in sporadic colorectal cancer tissues with that in HNPCC tissues. HNPCC patients were diagnosed based on Amsterdam criteria II, and paraffin-embedded tissues from sporadic colorectal cancers and HNPCCs were analyzed by immunohistochemistry with anti-lamin B2 antibody. The staining intensity of lamin B2 is objectively quantified using the TissueFAXS system and the corresponding HistoQuest software (TissueGnostics, Vienna, Austria). Sporadic colorectal cancer tissues showed lower levels of lamin B2 staining than HNPCC (Figures 7a and b; Table 1; Supplementary Figure S5), which supports the idea that repression of lamin B2 is involved in CIN. Interestingly, these data also showed that the mean intensity of lamin B2 expression in HNPCC (MIN) was 1.3 ± 0.4-hold higher than that in adjacent non-tumor tissues (Student's paired *t*-test, $P = 0.055$). These results suggest not only that a decrease in lamin B2 expression is involved in the induction

© 2014 Macmillan Publishers Limited

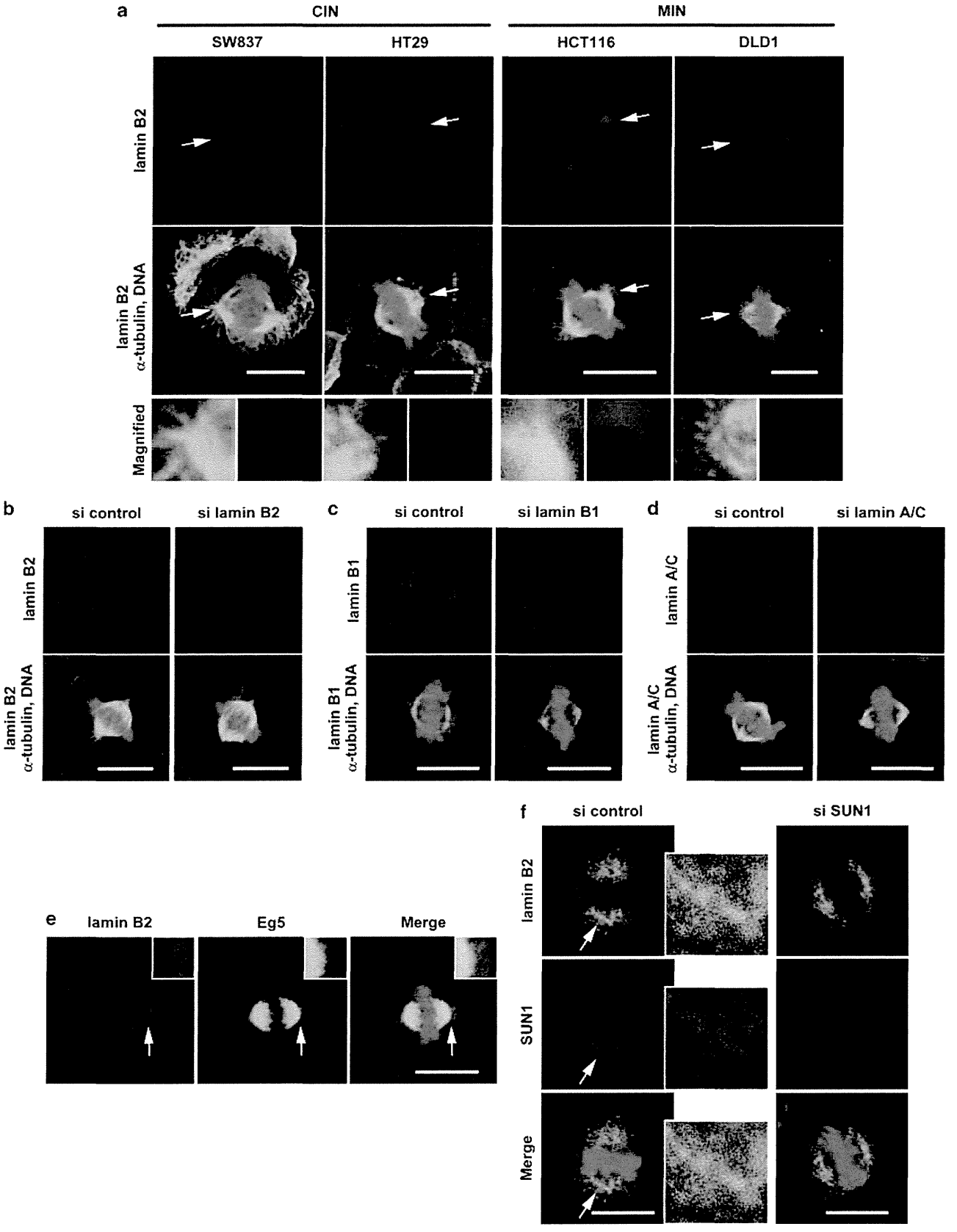


Figure 6. Disappearance of immunostaining for mitotic lamin B2 in CIN cell lines. (**a**) CIN (SW837 and HT29) and MIN (HCT116 and DLD1) cell lines were stained with anti-lamin B2 (red) and anti-α-tubulin (green) antibodies. Images show mitotic cells. (**b–d**, **f**) HCT116 cells were treated with siRNA targeting lamin B2 (**b**), B1(**c**) or A/C (**d**) or SUN1 (**f**) and stained with the indicated antibodies. (**e**) HCT116 cells were stained with anti-lamin B2 and anti-Eg5 antibodies. DNA was stained with DAPI (blue). Scale bars, 10 μm. The areas indicated by arrows are shown at high magnification.

© 2014 Macmillan Publishers Limited

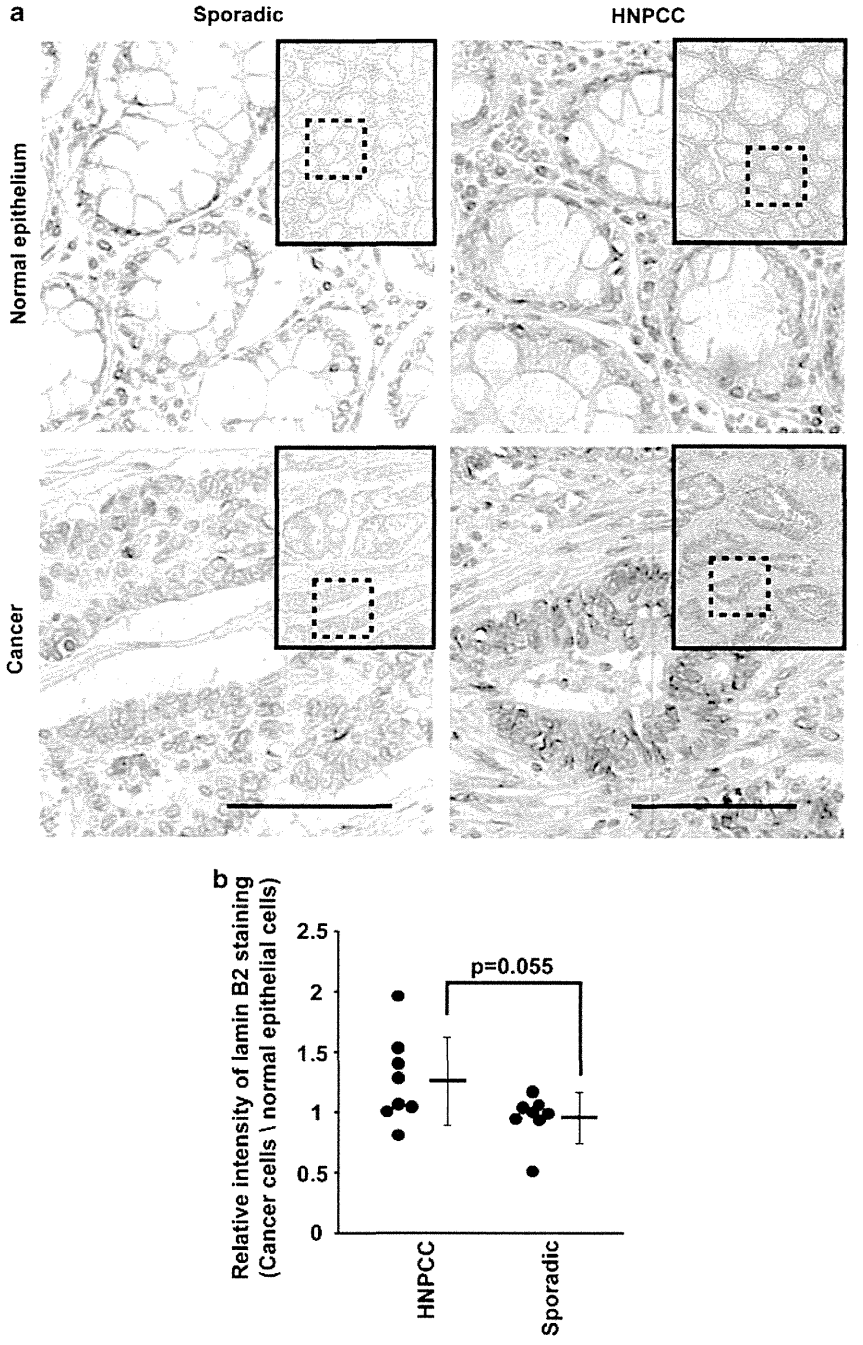


Figure 7. Immunohistochemical analysis of lamin B2 in sporadic colorectal cancer and HNPCC. Paraffin-embedded tissue sections of sporadic colorectal cancer (CIN) and HNPCC (MIN) were stained with rabbit polyclonal anti-lamin B2 antibody. Using the TissueFAXS system and HistoQuest software, images of cancer cells and adjacent normal epithelial cells in each tissue section were obtained, and the intensity of lamin B2 staining in these cells was quantitated. (**a**) Representative images at low and high magnification of the dotted square regions are shown. Bars, 100 μm. (**b**) Plot represents the value of the relative intensity of lamin B2 staining in cancer cells in each tissue section compared with the intensity in adjacent normal epithelial cells in the same tissue section, and the means ± s.d. are shown (sporadic colorectal cancer, $n = 8$; HNPCC, $n = 8$). The *P*-value was calculated by Student's *t*-test.

of CIN in human colorectal cancer but also that its enhanced expression might be required for MIN cancer to prevent CIN.

DISCUSSION

In this study, we provided the first evidence that downregulation of lamin B2 is involved in chromosome instability and that restoration of the lamin B2 level is able to prevent mitotic defects. Importantly, low levels of lamin B2 expression were observed not only in CIN colorectal cancer cell lines but also in sporadic colorectal cancer tissues (CIN). Furthermore, we determined a novel mitotic localization of lamin B2 outside the spindle poles. Our data suggest that lamin B2 has a critical role in preventing CIN in colorectal cancer by maintaining spindle pole stability and consequent spindle assembly.

The major cause of CIN is believed to be chromosome mis-segregation. Proper formation of bipolar spindles is crucial for accurate segregation of chromosomes.[4] Recent studies suggested

© 2014 Macmillan Publishers Limited

Table 1. Clinical features of patients with colorectal cancer

	Cancer type	*Age*	*Sex*	*Location*[a]	*Histological stage*	*Lamin B2 level*[a]
1	HNPCC	49	Male	R	3	1.4***
2	HNPCC	44	Male	S	4	1.0
3	HNPCC	46	Male	R	1	1.5***
4	HNPCC	44	Male	T	3	2.0***, 1.0[b]
5	HNPCC	57	Female	A	3	1.3***
6	HNPCC	48	Female	R	3	1.0
7	HNPCC	61	Female	A	2	0.8***
8	Sporadic	67	Male	T	3	0.9*
9	Sporadic	82	Male	A	2	1.2*
10	Sporadic	56	Female	A	3	1.0
11	Sporadic	67	Female	C	3	0.5***
12	Sporadic	41	Female	A	4	0.9
13	Sporadic	60	Male	S	3	1.1
14	Sporadic	67	Male	D,S	4	1.0
15	Sporadic	82	Male	D	2	1.0

Abbreviations: A, ascending colon; C, cecum; D, descending colon; R, rectum; S, sigmoid colon; T, traverse colon. Asterisks indicate significant differences between cancer and normal epithelial cells, calculated by Student's *t*-test (*$P<0.05$; ***$P<0.001$). [a]Levels of lamin B2 expression in cancer cells are relative to the adjacent normal epithelial cells (see Supplementary Figure S5). [b]Two distinct tissues from the same patient were examined for lamin B2 expression.

that B-type lamins associate with the mitotic spindle[25,26] and have an active role in mitotic progression by promoting the formation of a spindle matrix.[14,21] Furthermore, downregulation of lamin expression in *C. elegans* induced chromosome mis-segregation.[13] Intriguingly, in CIN colorectal cancer cell lines, lamin B2, but not lamins B1 and A/C, was specifically downregulated (Figure 1). Knockdown experiments of MIN colorectal cancer cells showed that decreased expression of lamin B2 is sufficient to cause aberrant spindle formation, chromosome mis-segregation and aneuploidy (Figures 2 and 3). These results suggest that lamin B2 is a cause of CIN in colorectal cancer.

Mitotic lamin B2 in MIN colorectal cancer cell lines was detected outside spindle poles (Figure 6a), although the previous report suggested that B-type lamins were co-localized with kinetochore microtubules in HeLa cells.[21] Mitotic lamin B2 staining outside the spindle poles was carefully confirmed using two different anti-lamin B2 antibodies and lamin B2 knockdown. The discrepancy might be explained by differences in cell lines or techniques of immunofluorescence.

This study further showed the co-localization of mitotic lamin B2 with an inner nuclear membrane protein SUN1 outside the spindle poles (Figure 6f). SUN1 is known to interact with outer nuclear membrane protein nesprins.[29,34] SUN1 and nesprins bind to lamins and cytoskeletal components, respectively, resulting in nuclear-cytoplasmic connection in interphase cells.[32] In addition, SUN1 was reported to mediate attachment of the nucleus to the centrosome in *C. elegans*.[31] These results indicate that the lamin–SUN1–nesprin complex stabilizes the position of the nucleus in a cell. Intriguingly, nesprin-2 and nesprin-3 were also identified by LC-MS/MS from lamin B2 immunoprecipitates prepared from mitotic HCT116 cells (Supplementary Table S1), suggesting that mitotic lamin B2 makes a complex with SUN1 and nesprins outside the spindle poles. Although the effect of the non-mitotic function of lamin B2 in mitotic processes is unknown, these results imply that the lamin B2 mitotic structure contributes to stabilization of the spindle poles and mitotic spindles.

As CIN is involved in tumorigenesis and tumor progression, prevention of CIN might be an approach for cancer therapy. A number of reports have shown that aberrant expression of mitotic proteins induces chromosome mis-segregation and causes CIN; however, it is unknown whether most of these proteins actively prevent mitotic defects. Recently, two microtubule-depolymerizing kinesins, Kif2b and MCAK, have been shown to actively prevent chromosome mis-segregation in CIN cancer cell lines.[35] Ectopic expression of these kinesins corrects improper microtubule attachment to kinetochores, leading to protection from chromosome mis-segregation. Our data showed that ectopic expression of lamin B2 in CIN cancer cells rescues aneuploidy and mitotic defects such as chromosome mis-segregation, mitotic delay and aberrant spindle formation (Figures 4 and 5), suggesting that forced expression of lamin B2 seems to promote the correction of chromosome segregation. Given that lamin B2 expression levels are enhanced in HNPCC MIN-type cancer as compared with not only CIN-type cancer but also non-tumor epithelium (Figure 7), enhanced lamin B2 expression in MIN cancer cells might be actively preventing CIN.

Our results may contribute to develop a novel strategy for cancer therapy that specifically targets aneuploid cancer cells. A recent report showed that proliferation of aneuploid, but not euploid, cancer cells is inhibited by AICAR, 17-AAG, chloroquine or their combination.[36] On the other hand, recent meta-analysis identified that MIN tumor patients do not benefit from fluorouracil-based adjuvant chemotherapy.[37] In this respect, determination of the state of chromosome stability of cancer may support a strategy for cancer therapy. Further study is needed to evaluate whether CIN-causative protein lamin B2 is a useful marker for planning a cancer therapy strategy as well as whether ectopic expression of lamin B2 is useful for CIN-preventing therapy.

MATERIALS AND METHODS

Cell culture and cell-cycle synchronization

Caco-2, HCT116, SW48, WiDr and RKO colorectal cancer cell lines were purchased from ATCC (Manassas, VA, USA). HT29 and SW480 cell lines and DLD1 and SW837 cell lines were kindly provided by Dr Takenaga and Dr Tagawa (Chiba Cancer Center Research Institute, Chiba, Japan), respectively. Cells were grown at 37 °C in 5% CO_2 in IMDM or RPMI-1640 (Invitrogen, Carlsbad, CA, USA) supplemented with 10% fetal bovine serum (Invitrogen) and 1% penicillin-streptomycin (Invitrogen). To accumulate mitotic cells, cells were pre-synchronized at the G_1/S phase upon treatment with 2 mM thymidine for 16 h and then released into fresh medium for 10–12 h.

Plasmid DNA, siRNA and antibodies

To generate lamin B2-GFP and lamin B2-mCherry plasmids, cDNA encoding human lamin B2 was amplified from HeLa cells by PCR using the forward primer 5′-TAAAGCTTATATGGCCACGCCGCTGCCC-3′ and the reverse primer 5′-ATAGGTACCCACATCACGTAGCAGCCTCTT-3′, and was cloned into pEGFP-N1 or pmCherry-N1 vector plasmids (Clontech, Palo Alto, CA, USA). To generate the mCherry-α-tubulin plasmid, full-length human α-tubulin cDNA was amplified from HeLa cells by PCR using the forward primer 5′-GCAAAGATCTATGCGTGAGTGCATCTCCATCC-3′ and the reverse primer 5′-GCGGGGATCCTTAGTATTCCTCTCCTTCTTC-3′, and was cloned into the pmCherry-C1 vector plasmid (Clontech). The histone H2B-GFP plasmid[38] was kindly provided by Dr Kimura (Kyoto University, Kyoto, Japan). Plasmids encoding lamin B2-shRNA (TRCN0000255440, TRCN0000255441, TRCN0000255443 and TRCN0000255444) or non-target control shRNA (SHC216) were purchased from Sigma-Aldrich (St Louis, MO, USA). Lamin B2-siRNA duplex (TCGGCAATAGCTCACCGTTTA) was purchased from Qiagen (Hilden, Germany) and Invitrogen (LMNB2-HSS189214). siRNA duplexes targeting lamins A/C (LMNA-HSS106094) and B1 (LMNB1-HSS106096) were purchased from Invitrogen. siRNA targeting SUN1 (Hs_UNC84A_2809) was purchased from Sigma-Aldrich. Control siRNAs were purchased from Qiagen (Firefly luciferase GL2-siRNA) and Invitrogen (Medium GC Duplex#2). Antibodies to the following proteins were purchased: mouse (LN43; Abcam, Cambridge, UK) and rabbit (Proteintech Group, Chicago, IL, USA) anti-lamin B2, goat anti-lamin B1 (sc-6216; Santa Cruz Biotechnology, Santa Cruz, CA, USA), mouse anti-lamin A/C (636; Santa Cruz Biotechnology), mouse (DM1A; Sigma-Aldrich) and rat (YOL1/34; Santa Cruz Biotechnology) anti-α-tubulin, mouse anti-β-tubulin

© 2014 Macmillan Publishers Limited

(TUB2.1; Sigma-Aldrich), mouse anti-GFP (Roche, Basel, Switzerland), rabbit anti-DsRed (Clontech), rabbit anti-KIF11 (Eg5) (HPA010568; Sigma-Aldrich), rabbit anti-SUN1 (sc-135077; Santa Cruz Biotechnology), and goat anti-actin (C-11; Santa Cruz Biotechnology) antibodies. Alexa Fluor 488 goat anti-mouse IgG and Alexa Fluor 594 goat anti-mouse IgG antibodies were purchased from Molecular Probes (Eugene, OR, USA). HRP-conjugated anti-mouse IgG (Dako, Glostrup, Denmark), anti-rabbit IgG (GE Healthcare, Little Chalfont, UK) and anti-goat IgG (MP Biomedicals, Santa Ana, CA, USA) antibodies were used.

Protein extraction and western blotting

Nuclear extracts were obtained from $\sim 1 \times 10^8$ cells. Cells were resuspended in 5 ml cold buffer (20 mM HEPES-KOH (pH 7.4), 20 mM KCl, 1 mM DTT, 0.1% NP-40, and Complete protease inhibitor cocktail; Roche) and allowed to swell on ice for 15 min. Then, cells were homogenized with a Dounce homogenizer or vigorously vortexed for 15 s 2 times and centrifuged for 5 min at 1000 r.p.m. After pellets were washed twice with the same cold buffer, they were solubilized in lysis buffer (7 M urea, 2 M thiourea, 4% w/v CHAPS, 30 mM Tris–HCl (pH 8.5) and Complete) by passing through 26-gauge needles and were then ultracentrifuged for 1 h at 100 000 *g*. For extraction of whole-cell proteins, cells were directly lysed in SDS–PAGE sample buffer. Western blotting was performed using the enhanced chemiluminescence (ECL) detection system (GE Healthcare), as described previously.[22,39]

RT–PCR

Extraction of total RNA and cDNA synthesis were performed as described previously.[40] The expression levels of lamin B2 mRNA were examined by PCR using the forward primer 5′-TCCGCACCGTCCTGGTTA-3′ and the reverse primer 5′-CCTGTTGGTGGAAAAGATCCTC-3′. The primer pair for GAPDH (RPP-401) was purchased from TOYOBO (Osaka, Japan).

Agarose 2D-DIGE and protein identification

Agarose 2D-DIGE was performed as described previously.[41] Pooled nuclear extracts (50 μg) of CIN cell lines (HT29, SW480, SW837 and Caco-2) and MIN cell lines (HCT116, RKO, DLD1 and SW48) were labeled with 400 pmol of Cy5 and Cy3, respectively. Internal standard, created by pooling aliquots of all the samples, was labeled with Cy2. The mixed labeled extract (50 μg each) was applied to agarose 2D-DIGE. In-gel tryptic digestion of proteins and identification by mass spectrometry were performed as described previously.[41,42]

Immunoprecipitation-LC-MS/MS

To collect mitotic HCT116 cells, cells were treated with 10 μM RO-3306 (Enzo Life Sciences, Farmingdale, NY, USA) for 19 h to arrest the cell cycle at G_2 phase and then cultured in fresh medium without the drug for further 45 min. To prepare cell lysates used for immunoprecipitation (IP lysates), cells were suspended in phosphate-buffered saline containing 1% NP-40, Complete, and phosphatase inhibitor cocktail PhosSTOP (Roche), and then homogenized by sonication. After centrifugation at 100 000 *g* for 30 min, the supernatant was collected. Immunoprecipitation was performed using anti-lamin B2 (LN43), A/C, or B1 antibody crosslinked to Protein G Dynabeads (Invitrogen) using dimethyl pimelimidate. IP lysates were reacted with antibody-coated Dynabeads for 1 h at 4 °C, and the absorbed proteins were eluted with SDS–PAGE sample buffer free of reducing agents. After reduction with β-mercaptoethanol, immunoprecipitates were resolved by SDS–PAGE and the gel lane was divided into several pieces, and in-gel tryptic digestion of proteins was performed as described previously.[43] The digested peptides were analyzed by LTQ-Orbitrap XL.[44] Protein identification was performed using the MASCOT search engine v2.4 (the UniProtKB/Swiss-Prot database 2012_6). Database search parameters were the charge of the precursor ion, 2+ and 3+; peptide mass tolerance, 3 p.p.m.; fragment tolerance, 0.6 Da; allowing up to one missed cleavage; fixed modification, carbamidomethylation of cysteine; variable modification, oxidation of methionine. Proteins were identified based on at least two unique peptides. The number of assigned spectra was calculated by the Scaffold 3 software (Proteome Software, Portland, OR, USA) for semiquantitation.

Immunostaining and FISH of cell lines

For immunostaining, cells were fixed with acetone for 10 min at 4 °C (Figures 1c and 3) or 4% HCHO for 20 min at room temperature (Figures 4d and e) or 30 °C (Figure 6), and HCHO-fixed cells were permeabilized in phosphate-buffered saline containing 0.5% Triton X-100 on ice. After blocking in phosphate-buffered saline containing 3% bovine serum albumin and 0.1% Tween-20, cells were stained with appropriate antibodies. Immunostained cells were viewed under an LSM710 confocal microscope with the Zen software (Carl Zeiss, Jena, Germany). The objective lenses were EC Plan-NEO FLUAR × 40/1.3 and Plan APOCHROMAT × 63/1.4. FISH was performed as described previously.[9,10] Probes to the pericentromeric regions of chromosome 7, 8, 12 and 15 were purchased from Vysis (Downers Grove, IL, USA). FISH-stained cells were viewed under a Zeiss fluorescent microscope with a × 40/1.3 or a × 63/1.4 oil immersion objective and an AxioVision digital imaging system (Carl Zeiss).

Transient and stable transfection

Transfection with plasmids or siRNA was performed using Lipofectamine 2000 or RNAiMAX (Invitrogen) as described previously.[9,10] For stable transfection, HCT116 or WiDr cells were transfected with histone H2B-GFP, mCherry-α-tubulin, lamin B2-shRNA, or control shRNA expression plasmid containing the neomycin- or puromycin-resistant gene and then selected in medium containing 400 μg/ml geneticin (Invitrogen) or 4 μg/ml puromycin (StressMarq Biosciences, Victoria, BC, Canada).

Live-cell imaging

Cells expressing histone H2B-GFP or mCherry-α-tubulin were mounted on a Zeiss LSM510 confocal microscope equipped with a heating stage (37 °C), CO_2 (5%) incubation chamber, and a × 40/1.2 water immersion or a × 63/1.4 oil immersion objective (Carl Zeiss). Cells were monitered at 3- or 5-min intervals. To detect the total fluorescence of histone H2B-GFP or mCherry-α-tubulin in a cell, z-stack images from the cell bottom to the cell top were collected and merged into a single plane at each time point during time-lapse experiments.

Patients and immunohistochemistry

From HNPCC and sporadic colorectal cancer patients, paraffin-embedded blocks of tumor tissues were collected in the Department of Frontier Surgery, Chiba University Hospital. The definition of HNPCC is based on the Amsterdam II criteria.[33,45] The ethics committee of the Graduate School of Medicine, Chiba University approved the protocol. Written informed consent was obtained from each patient before surgery. Four-micrometer sections from paraffin tissues were fixed on slide glasses. Tissues were immunostained as described previously.[46] After deparaffinization and antigen retrieval with microwave irradiation for 5 min in pH 6.0 citric buffer three times, tissues were stained using anti-lamin B2 antibody and En Vision + (Dako). Tissue sections were counterstained with hematoxylin. Using the TissueFAXS system and the corresponding HistoQuest software, stained tissues were viewed and lamin B2 staining was quantitated. Normal epithelial and cancer cells in at least 12 areas in each tissue section were analyzed for the mean intensity of lamin B2 staining, and the average value was calculated.

CONFLICT OF INTEREST

The authors declare no conflict of interest.

ACKNOWLEDGEMENTS

We would like to thank Hironori Funabiki for critical reading of this manuscript and Masumi Ishibashi for technical assistance. This work was supported by a Grant-in-Aid for Research on Biological Markers for New Drug Development H20-0005 to TT from the Ministry of Health, Labour and Welfare of Japan and by a Grant-in-Aid 21390354 to TT from the Ministry of Education, Science, Sports and Culture of Japan. This work was supported by a Grant-in-Aid for Research on Biological Markers for New Drug Development H20-0005 to TT from the Ministry of Health, Labour and Welfare of Japan and by a Grant-in-Aid 21390354 to TT from the Ministry of Education, Science, Sports and Culture of Japan.

REFERENCES

1 Lengauer C, Kinzler KW, Vogelstein B. Genetic instability in colorectal cancers. *Nature* 1997; **386**: 623–627.
2 Lengauer C, Kinzler KW, Vogelstein B. Genetic instabilities in human cancers. *Nature* 1998; **396**: 643–649.

© 2014 Macmillan Publishers Limited

3 Rajagopalan H, Lengauer C. Aneuploidy and cancer. *Nature* 2004; **432**: 338–341.
4 Holland AJ, Cleveland DW. Boveri revisited: chromosomal instability, aneuploidy and tumorigenesis. *Nat Rev Mol Cell Biol* 2009; **10**: 478–487.
5 Bischoff JR, Anderson L, Zhu Y, Mossie K, Ng L, Souza B *et al.* A homologue of Drosophila aurora kinase is oncogenic and amplified in human colorectal cancers. *EMBO J* 1998; **17**: 3052–3065.
6 Kops GJ, Weaver BA, Cleveland DW. On the road to cancer: aneuploidy and the mitotic checkpoint. *Nat Rev Cancer* 2005; **5**: 773–785.
7 Yuen KW, Montpetit B, Hieter P. The kinetochore and cancer: what's the connection? *Curr Opin Cell Biol* 2005; **17**: 576–582.
8 Zhou H, Kuang J, Zhong L, Kuo WL, Gray JW, Sahin A *et al.* Tumour amplified kinase STK15/BTAK induces centrosome amplification, aneuploidy and transformation. *Nat Genet* 1998; **20**: 189–193.
9 Tomonaga T, Matsushita K, Yamaguchi S, Oohashi T, Shimada H, Ochiai T *et al.* Overexpression and mistargeting of centromere protein-A in human primary colorectal cancer. *Cancer Res* 2003; **63**: 3511–3516.
10 Tomonaga T, Matsushita K, Ishibashi M, Nezu M, Shimada H, Ochiai T *et al.* Centromere protein H is up-regulated in primary human colorectal cancer and its overexpression induces aneuploidy. *Cancer Res* 2005; **65**: 4683–4689.
11 Tomonaga T, Nomura F. Chromosome instability and kinetochore dysfunction. *Histol Histopathol* 2007; **22**: 191–197.
12 Fawcett DW. On the occurrence of a fibrous lamina on the inner aspect of the nuclear envelope in certain cells of vertebrates. *Am J Anat* 1966; **119**: 129–145.
13 Liu J, Rolef Ben-Shahar T, Riemer D, Treinin M, Spann P, Weber K *et al.* Essential roles for Caenorhabditis elegans lamin gene in nuclear organization, cell cycle progression, and spatial organization of nuclear pore complexes. *Mol Biol Cell* 2000; **11**: 3937–3947.
14 Ma L, Tsai M-Y, Wang S, Lu B, Chen R, Yates III JR *et al.* Requirement for Nudel and dynein for assembly of the lamin B spindle matrix. *Nat Cell Biol* 2009; **11**: 247–256.
15 Maeshima K, Yahata K, Sasaki Y, Nakatomi R, Tachibana T, Hashikawa T *et al.* Cell-cycle-dependent dynamics of nuclear pores: pore-free islands and lamins. *J Cell Sci* 2006; **119**: 4442–4451.
16 Shaklai S, Amariglio N, Rechavi G, Simon AJ. Gene silencing at the nuclear periphery. *FEBS J* 2007; **274**: 1383–1392.
17 Shimi T, Pfleghaar K, Kojima S, Pack CG, Solovei I, Goldman AE *et al.* The A- and B-type nuclear lamin networks: microdomains involved in chromatin organization and transcription. *Genes Dev* 2008; **22**: 3409–3421.
18 Spann TP, Moir RD, Goldman AE, Stick R, Goldman RD. Disruption of nuclear lamin organization alters the distribution of replication factors and inhibits DNA synthesis. *J Cell Biol* 1997; **136**: 1201–1212.
19 Spann TP, Goldman AE, Wang C, Huang S, Goldman RD. Alteration of nuclear lamin organization inhibits RNA polymerase II-dependent transcription. *J Cell Biol* 2002; **156**: 603–608.
20 Stewart CL, Roux KJ, Burke B. Blurring the boundary: the nuclear envelope extends its reach. *Science* 2007; **318**: 1408–1412.
21 Tsai M-Y, Wang S, Heidinger JM, Shumaker DK, Adam SA, Goldman RD *et al.* A mitotic lamin B matrix induced by RanGTP required for spindle assembly. *Science* 2006; **311**: 1887–1893.
22 Kuga T, Nozaki N, Matsushita K, Nomura F, Tomonaga T. Phosphorylation statuses at different residues of lamin B2, B1, and A/C dynamically and independently change throughout the cell cycle. *Exp Cell Res* 2010; **316**: 2301–2312.
23 Maeshima K, Iino H, Hihara S, Funakoshi T, Watanabe A, Nishimura M *et al.* Nuclear pore formation but not nuclear growth is governed by cyclin-dependent kinases (Cdks) during interphase. *Nat Struct Mol Biol* 2010; **17**: 1065–1071.
24 Dechat T, Pfleghaar K, Sengupta K, Shimi T, Shumaker DK, Solimando L *et al.* Nuclear lamins: major factors in the structural organization and function of the nucleus and chromatin. *Genes Dev* 2008; **22**: 832–853.
25 Georgatos SD, Pyrpasopoulou A, Theodoropoulos PA. Nuclear envelope breakdown in mammalian cells involves stepwise lamina disassembly and microtubule-drive deformation of the nuclear membrane. *J Cell Sci* 1997; **110**: 2129–2140.
26 Maison C, Pyrpasopoulou A, Theodoropoulos PA, Georgatos SD. The inner nuclear membrane protein LAP1 forms a native complex with B-type lamins and partitions with spindle-associated mitotic vesicles. *EMBO J* 1997; **16**: 4839–4850.
27 Tsushimi T, Noshima S, Oga A, Esato K, Sasaki K. DNA amplification and chromosomal translocations are accompanied by chromosomal instability: analysis of seven human colon cancer cell lines by comparative genomic hybridization and spectral karyotyping. *Cancer Genet Cytogenet* 2001; **126**: 34–38.
28 Thompson SL, Compton DA. Examining the link between chromosomal instability and aneuploidy in human cells. *J Cell Biol* 2008; **180**: 665–672.
29 Crisp M, Liu Q, Roux K, Rattner JB, Shanahan C, Burke B *et al.* Coupling of the nucleus and cytoplasm: role of the LINC complex. *J Cell Biol* 2006; **172**: 41–53.
30 Haque F, Lloyd DJ, Smallwood DT, Dent CL, Shanahan CM, Fry AM *et al.* SUN1 interacts with nuclear lamin A and cytoplasmic nesprins to provide a physical connection between the nuclear lamina and the cytoskeleton. *Mol Cell Biol* 2006; **26**: 3738–3751.
31 Malone CJ, Misner L, Le Bot N, Tsai MC, Campbell JM, Ahringer J *et al.* The C. elegans hook protein, ZYG-12, mediates the essential attachment between the centrosome and nucleus. *Cell* 2003; **115**: 825–836.
32 Razafsky D, Hodzic D. Bringing KASH under the SUN: the many faces of nucleo-cytoskeletal connections. *J Cell Biol* 2009; **186**: 461–472.
33 Lynch HT, de la Chapelle A. Hereditary colorectal cancer. *New Engl J Med* 2003; **348**: 919–932.
34 Stewart-Hutchinson PJ, Hale CM, Wirtz D, Hodzic D. Structural requirements for the assembly of LINC complexes and their function in cellular mechanical stiffness. *Exp Cell Res* 2008; **314**: 1892–1905.
35 Bakhoum SF, Thompson SL, Manning AL, Compton DA. Genome stability is ensured by temporal control of kinetochore-microtubule dynamics. *Nat Cell Biol* 2009; **11**: 27–35.
36 Tang YC, Williams BR, Siegel JJ, Amon A. Identification of aneuploidy-selective antiproliferation compounds. *Cell* 2011; **144**: 499–512.
37 Des Guetz G, Schischmanoff O, Nicolas P, Perret GY, Morere JF, Uzzan B. Does microsatellite instability predict the efficacy of adjuvant chemotherapy in colorectal cancer? A systematic review with meta-analysis. *Eur J Cancer* 2009; **45**: 1890–1896.
38 Kanda T, Sullivan KF, Wahl GM. Histone-GFP fusion protein enables sensitive analysis of chromosome dynamics in living mammalian cells. *Curr Biol* 1998; **8**: 377–385.
39 Kuga T, Hoshino M, Nakayama Y, Kasahara K, Ikeda K, Obata Y *et al.* Role of Src-family kinases in formation of the cortical actin cap at the dorsal cell surface. *Exp Cell Res* 2008; **314**: 2040–2054.
40 Kuga T, Kume H, Kawasaki N, Sato M, Adachi J, Shiromizu T *et al.* A novel mechanism of keratin cytoskeleton organization through casein kinase Iα and FAM83H in colorectal cancer. *J Cell Sci* 2013; **126**: 4721–4731.
41 Nishimori T, Tomonaga T, Matsushita K, Oh-Ishi M, Kodera Y, Maeda T *et al.* Proteomic analysis of primary esophageal squamous cell carcinoma reveals downregulation of a cell adhesion protein, periplakin. *Proteomics* 2006; **6**: 1011–1018.
42 Tomonaga T, Matsushita K, Yamaguchi S, Oh-Ishi M, Kodera Y, Maeda T *et al.* Identification of altered protein expression and post-translational modifications in primary colorectal cancer by using agarose two-dimensional gel electrophoresis. *Clin Cancer Res* 2004; **10**: 2007–2014.
43 Adachi J, Kumar C, Zhang Y, Mann M. In-depth analysis of the adipocyte proteome by mass spectrometry and bioinformatics. *Mol Cell Proteomics* 2007; **6**: 1257–1273.
44 Narumi R, Murakami T, Kuga T, Adachi J, Shiromizu T, Muraoka S *et al.* A strategy for large-scale phosphoproteomics and SRM-based validation of human breast cancer tissue samples. *J Proteome Res* 2012; **11**: 5311–5322.
45 Vasen HF, Watson P, Mecklin JP, Lynch HT. New clinical criteria for hereditary nonpolyposis colorectal cancer (HNPCC, Lynch syndrome) proposed by the International Collaborative group on HNPCC. *Gastroenterology* 1999; **116**: 1453–1456.
46 Seimiya M, Tomonaga T, Matsushita K., Sunaga M, Oh-Ishi M, Kodera Y *et al.* Identification of novel immunohistochemical tumor markers for primary hepatocellular carcinoma; clathrin heavy chain and formiminotransferase cyclodeaminase. *Hepatology* 2008; **48**: 519–530.

Oncogenesis is an open-access journal published by *Nature Publishing Group*. This work is licensed under a Creative Commons Attribution-NonCommercial-NoDerivs 3.0 Unported License. To view a copy of this license, visit http://creativecommons.org/licenses/by-nc-nd/3.0/

Supplementary Information accompanies this paper on the Oncogenesis website (http://www.nature.com/oncsis)

© 2014 Macmillan Publishers Limited

Journal of proteome research

Article

pubs.acs.org/jpr

Absolute Quantitation of Low Abundance Plasma APL1β peptides at Sub-fmol/mL Level by SRM/MRM without Immunoaffinity Enrichment

Shozo Sano,[†] Shinji Tagami,[‡] Yuuki Hashimoto,[†] Kumiko Yoshizawa-Kumagaye,[§] Masahiko Tsunemi,[§] Masayasu Okochi,[‡] and Takeshi Tomonaga*[,†]

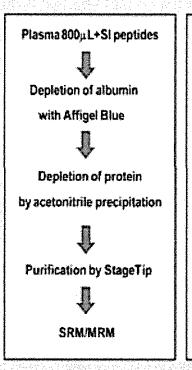
[†]Laboratory of Proteome Research, National Institute of Biomedical Innovation, Osaka 567-0085, Japan

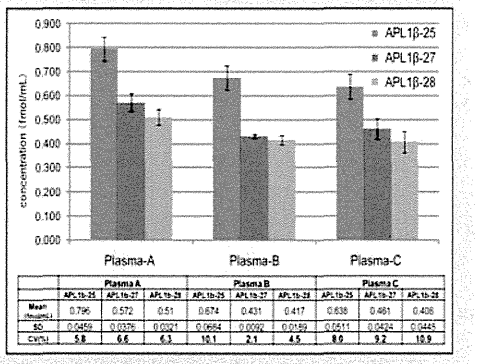
[‡]Psychiatry, Department of Integrated Medicine, Division of Internal Medicine, Osaka University Graduate School of Medicine, Osaka 565-0871, Japan

[§]Peptide Institute, Inc., Osaka 562-8686, Japan

S *Supporting Information*

ABSTRACT: Selected/multiple reaction monitoring (SRM/MRM) has been widely used for the quantification of specific proteins/peptides, although it is still challenging to quantitate low abundant proteins/peptides in complex samples such as plasma/serum. To overcome this problem, enrichment of target proteins/peptides is needed, such as immunoprecipitation; however, this is labor-intense and generation of antibodies is highly expensive. In this study, we attempted to quantify plasma low abundant APLP1-derived Aβ-like peptides (APL1β), a surrogate marker for Alzheimer's disease, by SRM/MRM using stable isotope-labeled reference peptides without immunoaffinity enrichment. A combination of Cibacron Blue dye mediated albumin removal and acetonitrile extraction followed by C_{18}-strong cation exchange multi-StageTip purification was used to deplete plasma proteins and unnecessary peptides. Optimal and validated precursor ions to fragment ion transitions of APL1β were developed on a triple quadruple mass spectrometer, and the nanoliquid chromatography gradient for peptide separation was optimized to minimize the biological interference of plasma. Using the stable isotope-labeled (SI) peptide as an internal control, absolute concentrations of plasma APL1β peptide could be quantified as several hundred amol/mL. To our knowledge, this is the lowest detection level of endogenous plasma peptide quantified by SRM/MRM.





KEYWORDS: *SRM/MRM, low abundant plasma peptide, peptide enrichment, Alzheimer's disease*

INTRODUCTION

Recent advances in proteomic technology have made it possible to quantitate biomarker candidate proteins/peptides using selected/multiple reaction monitoring (SRM/MRM), a very sensitive mass spectrometric technique for the detection and quantification of targeted proteins and peptides.[1] Suitable sets of precursor and fragment ion masses for a given peptide, called SRM/MRM transitions, constitute definitive mass spectrometry assays that identify peptides and the corresponding proteins. More recently, SRM/MRM using stable isotope peptides has been adapted to measure the concentrations of candidate protein/peptide biomarkers in cell lysates as well as human plasma and serum.[2−5]

Although SRM/MRM is a very sensitive mass spectrometric technique, human plasma and serum are the most challenging biospecimens for the detection and quantitation of protein/peptide biomarkers due to highly abundant proteins such as albumin and immunoglobulin that impede the detection of low abundant proteins/peptides. A common approach to deplete plasma/serum abundant proteins is the use of immunodepletion, which specifically removes high abundance proteins such as albumin, transferrin, and immunoglobulins. Although previous reports efficiently removed high abundance plasma proteins using IgY14 or SuperMix,[6,7] other highly abundant proteins still existed in the flow-through fraction. Therefore, an additional enrichment step must be added to quantify candidate biomarkers present at lower concentrations in plasma/serum. Targeted enrichment has been performed with or without antibodies to improve the sensitivity of quantitation. Recently, a combination of the immunoaffinity approach with SRM/MRM using stable isotope peptides, such as SISCAPA-SRM, immuno-SRM, and mass spectrometric immunoassay (MSIA), significantly improved the quantification of low abundant protein

Received: October 8, 2013

ACS Publications © XXXX American Chemical Society

biomarkers present in plasma.[8−13] Using the MSIA method, the lowest detection level (LOQ) of plasma proteins is 16−31 pg/mL.[13] However, antibodies of proteins/peptides of interest are not always commercially available and there is no guarantee of being able to obtain suitable antibodies for immunoprecipitation if they are developed in-house. Therefore, antibody-free enrichment of target proteins has recently been applied for the quantitation of low abundant plasma proteins and demonstrated accurate and reproducible quantification of proteins at concentrations in the 50−100 pg/mL range.[14]

A key feature of the pathology of Alzheimer's disease (AD) is the accumulation of amyloid-β peptides (Aβ) in senile plaques and Aβ42 is its major constituent.[15,16] Thus, the level of Aβ42, especially relative to total Aβ in the brain, is a potential biomarker of AD. However, since Aβ42 is cleared more rapidly from the soluble pool in the brain by an enhanced rate of deposition/aggregation,[17−19] it is hardly detected in body fluid such as CSF and plasma, and surrogate markers for estimating Aβ42 generation in the brain have not yet been identified. We have previously identified novel APLP1-derived Aβ-like (APL1β) peptides, APL1β 25, 27, 28, that consist of 25−28 amino acids, in human CSF[20,21] and demonstrated that the CSF APL1β28 level is a potential surrogate marker for brain Aβ42 production. Moreover, the relative APL1β28 level as compared with total APL1β peptides is higher in CSF from sporadic AD patients than from non-AD controls, which is a potential biomarker for AD. However, examination of CSF is highly invasive for medical screening and a less aggressive procedure such as a blood test is needed.

Various methods have been used to analyze low molecular weight peptides in plasma/serum, including ultrafiltration, organic precipitation, and solid-phase extraction cartridges.[22−25] However, the most suitable method for analysis depends on the peptides to be analyzed. Several endogenous peptides in plasma or serum, such as human parathyroid hormone, insulin, and gastric inhibitory polypeptides, have been recently quantified by SRM/MRM, and the LOQ of the peptides was 1−18 fmol/mL.[26−28] In this study, we combined Cibacron Blue F3GA dye mediated albumin removal (Affi-Gel Blue; Bio-Rad, Hercules, CA) and acetonitrile (ACN) extraction to deplete plasma/serum proteins for SRM/MRM analysis of APL1β peptides. We also used C18-SCX multi-StageTips for removing unnecessary peptides.[29] Using 800 μL of plasma, endogenous APL1β peptides were able to be detected and quantified by SRM/MRM without immunoaffinity enrichment of the peptides. Strikingly, the absolute concentration of APL1β peptides was identified as several hundred amol/mL, which is the lowest detection level of endogenous plasma peptides to our knowledge.

MATERIALS AND METHODS

Synthetic Peptides

APL1β25, 27, 28 synthetic peptides were described previously.[21] Stable isotope-labeled peptides (SI peptides) for APL1β25, 27, 28 with a ^{15}N- and ^{13}C-labeled leucine[3] were synthesized at the Peptide Institute, Inc. (Osaka, Japan) using the t-butyloxycarbonyl (Boc) strategy and purified by reversed-phase (RP) HPLC. The labeled starting material, Boc-Leu(U−$^{13}C_6$, ^{15}N) (isotopic purity: 98%), was purchased from Cambridge Isotope Laboratories (Andover, MA). The chemical purity of these peptides was more than 98% determined by RP-HPLC and/or by capillary zone electrophoresis. The exact quantities of the synthetic peptides were determined by amino acid analysis of their acid hydrolysates in order to apply them to absolute quantitation of APL1β peptides in human plasma.

Collection of Human Plasma

Blood samples were collected from healthy volunteers at Osaka University Hospital. All the experiments using plasma were approved by the ethics committee of Osaka University Hospital (Nos. 07139 and 07212). Blood samples were centrifuged for 10 min at 3000*g*, and aliquots of the plasma supernatants were frozen immediately at −80 °C. The plasma samples were frozen and thawed once or twice before measurement.

Pretreatment of Plasma, Albumin Depletion, and ACN Precipitation

Human plasma samples were pretreated using Affi-Gel Blue and Mini Bio-Spin Chromatography Columns (Bio-Rad, Hercules, CA) according to the manufacturer's instructions. Briefly, 800 μL of plasma was diluted with an equal volume of 25 mM K_2HPO_4 and 0.1% *n*-octyl-β-glucoside (pH 7.0), and the SI peptide mixture was added to the pretreated samples at 5 fmol/mL. The sample was loaded onto a 1 mL Affi-Gel Blue column and vigorously mixed for 10 min at room temperature. The column was centrifuged for 1 min at 10 000*g*, and the eluate was applied to a new Affi-Gel Blue column, vigorously mixed for 10 min at room temperature, and centrifuged, and then the eluate was collected.

ACN was added to the eluate at several concentrations, as indicated in the text and in Figure 2, and centrifuged for 10 min at 20 000*g*. The supernatant was dried with a SpeedVac and resuspended with 100 μL of 40% ACN and 0.1% trifluoroacetic acid (TFA) and incubated for 3 or 5 min at room temperature. The sample was diluted with an equal volume of distilled water and centrifuged for 10 min at 20 000*g*. A volume of 5 μL of TFA was added to the supernatant and subjected to the following procedures.

StageTip Purification of Pretreated Plasma

To make the C_{18}-SCX multi-StageTip, a small portion of Empore Cation-SR Disk (3 M Company, St. Paul, MN) and C_{18} Disk, one disk per 10 μg of protein, were laminated in multiple in ordinary pipet tips. The StageTip was washed with 100% methanol, 80% ACN + 0.1% TFA, 2% ACN + 0.1%TFA, 500 mM ammonium bicarbonate + 30% ACN + 0.1% TFA, 2% ACN + 0.1% TFA, 80% ACN + 0.1% TFA, and 2% ACN + 0.1% TFA again. A pretreated plasma sample with Affi-Gel Blue and ACN precipitation was loaded onto the C_{18}-SCX multi-StageTip and washed with 2% ACN + 0.1% TFA. Then, APL1β peptides were eluted from the C_{18} disk with 120 μL of 80% ACN + 0.1% TFA to transfer to a cation-exchange disk. The StageTip was washed with 2% ACN + 0.1% TFA and 10 mM ammonium bicarbonate + 30% ACN + 0.1% TFA, and then APL1β peptides were eluted with 120 μL of 20 mM ammonium bicarbonate + 30% ACN + 0.1% TFA. The eluate was dried with a SpeedVac and resuspended in 25 μL of 20% acetonitrile and 0.1% TFA, and then 20 μL was analyzed with LC-MS/MS.

Setting of SRM/MRM Transition

SRM/MRM analysis was performed as previously described.[30] First, the mixture of endogenous and SI APL1β peptides was analyzed by LC-MS/MS using LTQ-Orbitrap Velos to acquire MS and MS/MS data (Supporting Information Figure 1). A preliminary SRM/MRM transition list for the peptides was

created from this acquired MS data using Pinpoint ver.1.0 (Thermo Fisher Scientific, Bremen, Germany). Then, the APL1β peptide mixture was analyzed using a TSQ-Vantage triple quadruple mass spectrometer (Thermo Fisher Scientific) with a nano-LC interface (AMR, Tokyo, Japan), Paradigm MS2 (Michrom Bioresources, Auburn, CA) and HTC PAL autosampler (CTC Analytics, Zwingen, Switzerland). The obtained data were analyzed using Pinpoint software to optimize parameters such as the collision energy (CE) and to acquire the retention times of each APL1β peptide. Finally, optimal transitions per peptide were selected for quantitation using SRM/MRM analysis (Table 1, Figure 2).

For the quantitation of plasma APL1β peptides by SRM/MRM, pretreated plasma dissolved in 20% acetonitrile and 0.1% TFA was analyzed by the above-mentioned optimal-timed SRM/MRM using TSQ-Vantage. SI peptide mixture was added to the pretreated samples at 5 fmol/mL, and endogenous peptides were quantified against spiked internal standard SI peptides. The flow rate of nanoLC was 500 nL/min and a linear gradient of ACN concentration was developed from 5 to 55% in several time windows, as indicated in the text and Figure 3. A spray voltage of 1900 V was applied. Data were acquired in nontime-scheduled SRM/MRM mode.

Data Analysis

APL1β peptides were quantitated using Pinpoint software. The peak area in the chromatogram of each SRM/MRM transition was measured and the amount of targeted peptides was calculated based on the peak area of the corresponding internal standard peptides. Final concentration of target peptides was determined as the average of all SRM/MRM transitions. The limits of detection (LODs) and quantification (LOQs) were determined as previously reported.[31]

RESULTS

Synthesis of Stable Isotope-Labeled Internal Standards APL1β peptides and Development of Transitions for SRM/MRM Analysis

For accurate quantitation of target peptides with SRM/MRM, stable isotope-labeled peptides (SI peptides) were used as internal standards. Thus, we synthesized nonlabeled and SI peptides for APL1β 25, 27, 28. The chemical purity of these peptides was more than 98% determined by RP-HPLC and/or by capillary zone electrophoresis. The exact quantities of the synthetic peptides were determined by amino acid analysis of their acid hydrolysates in order to apply them for absolute quantitation of APL1β peptides in human plasma. Also, full MS/MS spectra were obtained for sequence confirmation (Supporting Information Figure 1). Next, the SRM/MRM transitions and collision energy (CE) were generated for each targeted peptide (Table 1). The SI peptide standards were subsequently analyzed by monitoring the selected transitions, and visual inspection of the SRM/MRM transition peak was performed (Figure 1).

Depletion of Plasma Proteins and Unnecessary Peptides by Combination of Affi-Gel Blue, ACN Precipitation, and Multi-StageTips

For detection of low abundant plasma proteins by mass spectrometry, proteins need to be digested with proteases such as trypsin after enrichment of target proteins. However, tryptic digestion is not necessary to detect low abundant endogenous

Table 1. List of Transitions for SRM/MRM Analysis of APL1β Peptides

		endogenous						SI					
peptide	sequence	parent ion (m/z)	ion charge state	fragment ion (m/z)	ion charge state	ion type	CE	parent ion (m/z)	fragment ion (m/z)	ion charge state	ion type	CE
APL1β-25	DELAPAGTGVSREAVSGLLIMGAGG	776.734	3	969.020	2	b20	40	779.073	972.529	2	b20	41
				912.478	2	b19	40		915.987	2	b19	41
				392.159	1	y5	40		392.159	1	y5	41
				950.500	2	y21	40		950.500	2	y21	41
APL1β-27	DELAPAGTGVSREAVSGLLIMGAGGGS	824.751	3	969.020	2	b20	45	827.091	972.529	2	b20	45
				1022.528	2	y23	45		1022.528	2	y23	45
				912.478	2	b19	45		915.9868	2	b19	45
				1034.540	2	b21	45		1038.040	2	b21	45
APL1β-28	DELAPAGTGVSREAVSGLLIMGAGGGSL	862.446	3	912.478	2	b19	49	864.785	915.987	2	b19	49
				969.020	2	b20	49		972.529	2	b20	49
				1034.541	2	b21	48		1038.049	2	b21	48

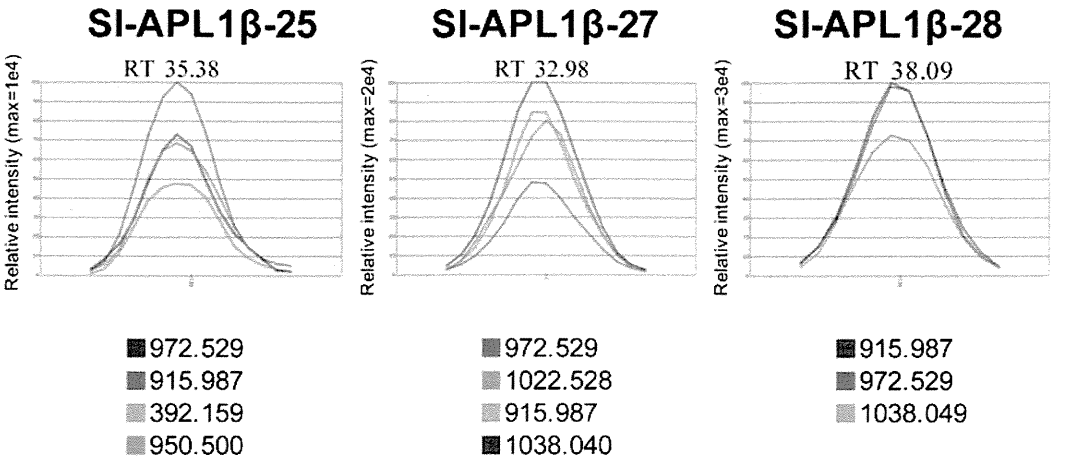


Figure 1. Peak shapes of selected transitions of SI APL1β peptides. See Table 1 for details of peptides. Retention time is shown as RT.

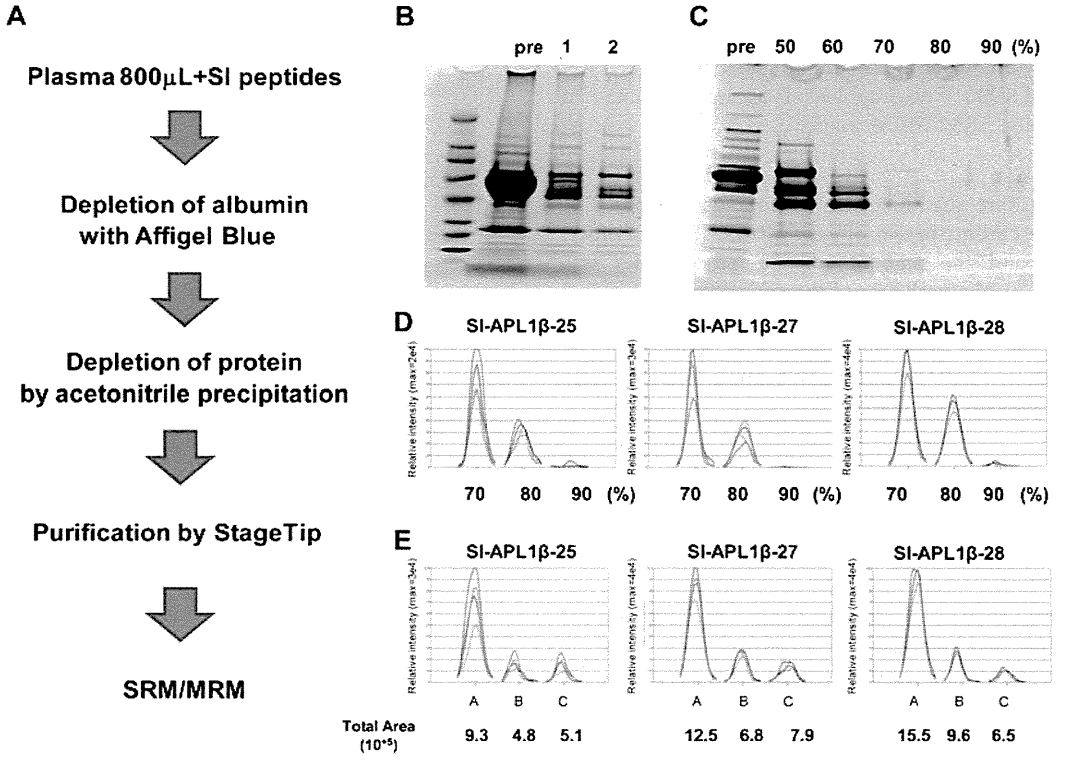


Figure 2. Depletion of plasma proteins and unnecessary peptides by combination of Affi-Gel Blue, ACN precipitation. and multi-StageTips. (A) Outline of the experimental workflow. (B) Depletion of plasma albumin using Affi-Gel Blue: pre, before depletion; 1, Affi-Gel Blue treatment once; 2, Affi-Gel Blue treatment twice. (C) Depletion of plasma proteins by different concentrations (50–90%) of acetonitrile precipitation: pre, untreated crude plasma. SDS-PAGE corresponding 0.02 μL plasma showed that most plasma proteins were depleted by >70% acetonitrile concentration. (D) Transition peaks of SI APL1β peptides spiked at the concentration of 5 fmol/mL after different concentrations (70–90%) of acetonitrile precipitation. Peak intensities were highest in the supernatant with 70% ACN precipitation and gradually decreased as ACN concentration increased. (E) Transition peaks of SI APL1β peptides spiked at the concentration of 5 fmol/mL after different plasma protein depletion methods. A: Combination of Affi-Gel Blue and ACN precipitation followed by StageTip purification. B: 70% ACN precipitation followed by StageTip purification. C: Ultrafiltration followed by StageTip purification. Total area of all transition peaks is shown. The combination of Affi-Gel Blue and ACN precipitation showed highest peak areas among the methods examined.

plasma peptides. Instead, removal of as much plasma proteins as possible is crucial.

To deplete most of the plasma proteins and enrich peptides efficiently, we used several methods. First, we tried 70% ACN precipitation or ultrafiltration (50 kDa MWCO) for depletion of plasma proteins and simultaneous recovery of APL1β peptides. The amount of APL1β peptides quantitated by SRM/MRM was lower after depletion of plasma proteins with 70% ACN precipitation and ultrafiltration as compared with combination with Affi-Gel Blue and ACN precipitation (data shown in Figure 2E), probably because APL1β peptides were captured with depleted or precipitated plasma proteins. Thus, we first depleted the most abundant plasma protein, albumin, with Cibacron Blue F3GA dye and subsequently depleted

residual plasma proteins with 70% ACN (Figure 2A). Eight hundred microliters of plasma diluted with an equal volume of Affi-Gel Blue depletion buffer were subjected to Affi-Gel Blue. The Coomassie Blue stained band corresponding to albumin in SDS-PAGE gel was almost abolished by two rounds of Affi-Gel Blue treatments (Figure 2B). Subsequently, ACN was added to the flow through to a final concentration of 50–90% and centrifuged to precipitate proteins. The supernatant was dried with SpeedVac and resuspended in 200 μL of 20% ACN and 0.1% TFA. SDS-PAGE analysis of the supernatant showed residual Coomassie Blue-stained bands in the supernatant of 50 and 60% ACN precipitation, whereas faint bands in the supernatant of >70% ACN precipitation (Figure 2C).

Unnecessary proteins/peptides were further depleted by passing through multi-StageTips containing reversed phase and cation-exchange materials. StageTips were developed by inserting Empore disks, chromatographic beads immobilized between Teflon meshworks, in an ordinary pipet tip.[29] Multi-StageTips were made by placing a combination of disks containing beads with different surfaces, which enabled 2D fractionation. We used C_{18}-SCX multi-StageTips to enrich APL1β peptides by organic solvent-based and strong cation fractionation. APL1β peptides bound to the StageTip were eluted with 20 mM ammonium bicarbonate, 30% ACN and 0.1% TFA, dried with SpeedVac, resuspended in 20% ACN and 0.1% TFA, and analyzed by SRM/MRM.

We examined peak areas of SI APL1β peptides spiked at the concentration of 5fmol/mL after treatment with ACN precipitation followed by StageTip purification. The peak areas were highest in the supernatant of 70% ACN precipitation and thus we decided to precipitate with 70% ACN (Figure 2D).

To investigate the recovery of APL1β peptides using different peptide enrichment procedures, we compared peak areas of SI APL1β peptides after the combination of Affi-Gel Blue and ACN precipitation with those treated with 70% ACN precipitation and ultrafiltration. As expected, peak areas of SI APL1β peptides using the combination of Affi-Gel Blue and ACN precipitation were 1.61–1.94 times and 1.58–2.38 times higher than 70% ACN precipitation and ultrafiltration, respectively (Figure 2E).

Evaluation of Recovery Efficiency of Plasma APL1β Peptides in the Sample Preparation Procedure

Recovery efficiency of plasma APL1β peptides in the sample preparation is crucial for the sensitivity of the assay. Thus, we assessed the recovery efficiency of plasma APL1β at each step of the workflow using SI peptides. The recovery was determined by measuring the relative amount of SI APL1β peptides before and after each step of the workflow. SI peptides were spiked into plasma, Affi-Gel Blue treated sample, Affi-Gel Blue treated and 70% ACN-precipitated sample, and the sample after StageTip purification at the concentration of 1 fmol/mL. Then, the relative peak area ratio of SI peptides before and after each step was compared to estimate the recovery efficiency. Recovery rates of APL1β peptides ranged from 71.7 to 86.0% after Affi-Gel Blue treatment, 69.3–83.4% after Affi-Gel Blue treatment and 70% ACN precipitation, and 50.2–64.0% after the overall procedure (Table 2).

Table 2. Recovery Efficiency of Plasma APL1β Peptides in the Sample Preparation Procedure

	before	Affi-Gel Blue	Affi-Gel Blue ACN precipitation	Affi-Gel Blue ACN precipitation Stage-Tip
APL1β-25	100.00%	77.40%	76.90%	64.00%
APL1β-27	100.00%	71.70%	69.30%	50.20%
APL1β-28	100.00%	86.00%	83.40%	54.60%

Optimization of LC Gradient

SRM/MRM with SI internal standards peptides is a highly accurate quantitative method for peptides; however, problems with coeluting interference frequently occur. The key factors contributing to interference are the components of highly complex samples, such as plasma, referred to as biological "noise". To eliminate biological interference, we extended the separation time of LC, a gradient from 5% to 55% of ACN, from 20 to 120 min and examined the effect on interference. Supporting Information Figure 2 shows an example. Strikingly, a single peak observed with 20-min separation became a double peak when the separation time was extended to >40 min and the peak observed later was identified as a background peak of the sample. Thus, extension of the LC separation time was very effective to eliminate biological interference.

To shorten the total separation time of LC, we increased the gradient rapidly from 5% to 15% in one minute and then slowly from 15% to 30% in 35 min. The peak areas of APL1β peptides were comparable with those using 120-min separation (data not shown). Thus, we used the above LC separation method for the following experiments.

LODs and LOQs of APL1β Peptides in Human Plasma

To examine the performance of our SRM/MRM assay, we evaluated the linear range, limits of detection (LODs), and quantitation (LOQs). The target SI peptides were spiked into 800 μL human plasma at nine different concentrations from 0 to 10 fmol, while nonlabeled synthetic peptides were spiked at a concentration of 10 fmol/mL in each sample as an internal standard. The concentration of target SI peptides at each concentration point was calculated based on the peak area of the corresponding internal standard peptides and determined as the average of all SRM/MRM transitions. Technical replicates were performed in triplicate at the nine concentration points. The linear correlation between the peak area ratios of the spiked SI peptides was obtained for each transition monitored over the 3 orders of magnitude, spanning peptide concentrations of 0.075–10 fmol/mL, measured in the experiment (R^2 > 0.99) (Figure 3), which indicates that the target peptides were able to be quantified without interference from the endogenous peptide or passenger peptide. This also allowed for the characterization of LODs and LOQs, which was determined as average blank measurements +3 and 10 times SD, respectively, calculated based on the peak area of nonlabeled internal standard peptides, as previously reported.[31] LODs and LOQs corresponding to APL1β differed between the transitions used and were 0.095–0.227 and 0.237–0.632 fmol/mL for APL1β 25, 0.131–0.278 and 0.318–0.734 fmol/mL for APL1β 27, and 0.076–0.162 and 0.152–0.342 fmol/mL for APL1β 28 (Table 3). Importantly, coefficients of variance (CVs) of the peak area between measurements (n = 3) often fell below 20% under the LOQ level (Figure 3). Schoenherr et al. used the lowest points above LOD with CV < 20% as LOQ.[32] Thus, we also defined LOQ as the lowest point of the spiked APL1β 25, 27, 28 peptides with CV < 20% between measurements above LOD, which was 0.3 fmol/mL (<1 pg/mL) (Figure 3). This LOQ was much lower than that of previously reported plasma gastric inhibitory polypeptide quantitation (1–10 fmol/mL).[28]